

Supporting Information

Switching Acidic and Basic Catalysis in a Three-Dimensional Covalent Imine Structure through Supramolecular Functionalization

Javier Luis-Barrerra, Rafael Cano, Ghazaleh Imani-Shakibaei, Javier Heras-Domingo, Javier Pérez-Carvajal, Inhar Imaz, Daniel Maspoch, Xavier Solans-Monfort, José Alemán,* and Rubén Mas-Ballesté**

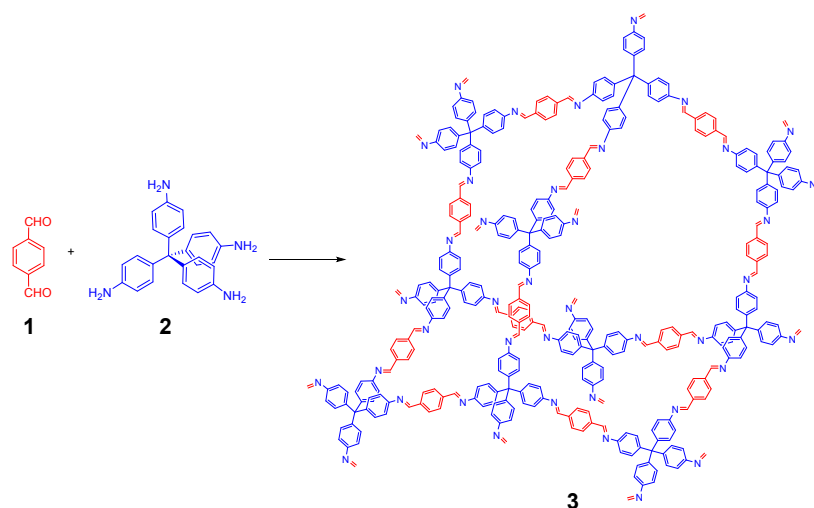
Table of Contents

1.	Materials and methods	S2
1.1	Synthesis of the materials	S2
2.	Powder XRD diffractograms	S4
3.	SEM images for a-3 materials and particle size distribution	S6
4.	NMR spectra of the materials	S8
5.	IR spectra	S9
6.	TGA-MS	S11
7.	General procedure for the catalysis with COF and characterization of products	S21
7.1	Epoxide opening catalyzed by COF	S21
7.2	Knoevenagel condensation catalyzed by COF	S23
7.3	Formation of 9g catalyzed by COF and by NEt ₃	S25
7.4	Epoxide opening and Knoevenagel background reactions	S27
8.	Calculation of chemical erosion of COF	S28
9.	COF stability after reactions	S38
10.	Leaching tests	S41
11.	¹ H-NMR spectra of products	S44
12.	Computational details	S50

1. Material and methods

All reagents for the synthesis of materials and for the catalyzed reactions and all organic solvents were acquired from commercial sources and used without further purification. Flash column chromatography was performed using pore 60 Å, 40-63 μm silica gel and compressed air. NMR spectra were acquired on a *Bruker Avance 300* spectrometer, running at 300 MHz for ¹H. Chemical shifts (δ) are reported in ppm relative to residual solvent signals (CDCl₃, 7.26 ppm for ¹H-NMR). The following abbreviations are used to describe peak patterns when appropriate: s (singlet), d (doublet), t (triplet), q (quartet), quint (quintet), m (multiplet), bs (broad singlet). Solid NMR spectra were acquired on a *Bruker AV 400 WB* spectrometer, running at 100 MHz for ¹³C. Scanning Electron Microscopy (SEM) images were acquired in a *Philips XL30 S-FEG* microscope and the samples surfaces were previously metalated with chromium with a *Sputter Coater Quorum, Q150T-S*. Infra Red (IR) spectra were acquired in a *Agilent Technologies Cary 630 FTIR* spectrometer. PXRD patterns were collected with a *Bruker D8 Advance* X-ray diffractometer (Cu-Kα radiation; λ = 1.5418 Å) equipped with a Lynxeye detector. Samples were mounted on a flat glass plate. Patterns were collected in the 5° < 2θ < 100° range with a step size of 0.02° and exposure time of 0.5 s/step. Thermogravimetric analysis (TGA) was done in a *TGA Q500 TA Instruments* thermobalance coupled to a *ThermoStar* mass spectrometer. The yield of the catalyzed reactions was measured by gas chromatography (GC) using an *Agilent Technologies 7820A GC System* with a Flame Ionization Detector (FID). Volumetric N₂ sorption isotherms were collected at 77 K (liquid N₂) using an ASAP 2020 HD (Micromeritics). Temperature was controlled by using a liquid nitrogen bath.

1.1. Synthesis of the materials



1.1.1. Synthesis of CH₃COOH@a-3

A round-bottom flask was charged with 20 mL of dichloromethane, 3 mL of glacial acetic acid and 28.8 mg of tetrakis(4-aminophenyl)methane **2** (0.075 mmol), and the resulting mixture was stirred during 30 minutes. The solution was filtered through filter paper in order to remove particles that are not solved. In another flask, 20.1 mg of 1,4-benzendicarbaldehyde **1** (0.150 mmol) was dissolved in 15 mL of dichloromethane. The solution of 1,4-benzendicarbaldehyde **1** was added to the solution of tetrakis(4-aminophenyl)methane **2**, and it was stirred during 2 hours at room temperature. After this period, the precipitated yellow solid was filtrated through a membrane filter of 0.45 µm pores and washed with 10 mL of water, 10 mL of acetone and 5 x 10 mL of dichloromethane. It was obtained 40 mg of CH₃COOH@a-3 (93%).

1.1.2. Synthesis of evacuated a-3

A round bottom flask was charged with 40 mg of CH₃COOH@a-3. Vacuum was then applied to the flask while heating at 80° C during 12 hours.

1.1.3. Synthesis of evacuated c-3

A solvothermal reactor was charged with 116 mg of CH₃COOH@a-3, 10.5 mL of 1,4-dioxane, 3.1 mL of glacial acetic acid, 2.1 mL of water and 2.1 mL of mesitylene. The mixture was heated under solvothermal conditions from 25 °C to 120 °C during 1 hour, and then to 120 °C during 7 days. The solution was then cooled down to room temperature (from 120 °C to 25 °C in 1 hour). The precipitated solid was filtered through a membrane filter of 0.45 µm pores, washed with 10 mL of water, 10 mL of acetone and 5 x 10 mL of dichloromethane, and placed in a flask where it was heated at 80 °C under vacuum for 12 hours to obtain 100 mg of evacuated c-3 (88%).

1.1.4. Synthesis of crystalline CH₃COOH@c-3

100 mg of evacuated c-3 were added to a mixture of dichloromethane (50 mL) and CH₃COOH (7.5 mL), and the resulting mixture was stirred during 12 hours. The solid was then filtrated through a membrane filter of 0.45 µm pores and washed with 10 mL of water, 10 mL of acetone and 5 x 10 mL of dichloromethane to obtain 104 mg of CH₃COOH@c-3 (89%).

1.1.5. Synthesis of Et₃N@a-3 and Et₃N@c-3

A round-bottom flask was charged with 40 mg of **evacuated a-3** or **c-3** and 4 mL of NEt₃. The flask was connected to a water-cooled condenser and it was warmed to 80° C during 12 hours. The solid was filtrated through a membrane filter of 0.45 μm pores and washed with 10 mL of water, 10 mL of acetone and 5 x 10 mL of dichloromethane to obtain 35 mg of the material (86%).

1.1.6. Synthesis of CH₃COOH···NEt₃@a-3 and CH₃COOH···NEt₃@c-3

A round-bottom flask was charged with 40 mg of **CH₃COOH@a-3** or **CH₃COOH@c-3** and 4 mL of NEt₃. The flask was connected to a water-cooled condenser and it was warmed to 80° C during 12 hours. The solid was filtrated through a membrane filter of 0.45 μm pores and washed with 10 mL of water, 10 mL of acetone and 5 x 10 mL of dichloromethane to obtain 33 mg of the material (92%).

2. Powder XRD diffractograms

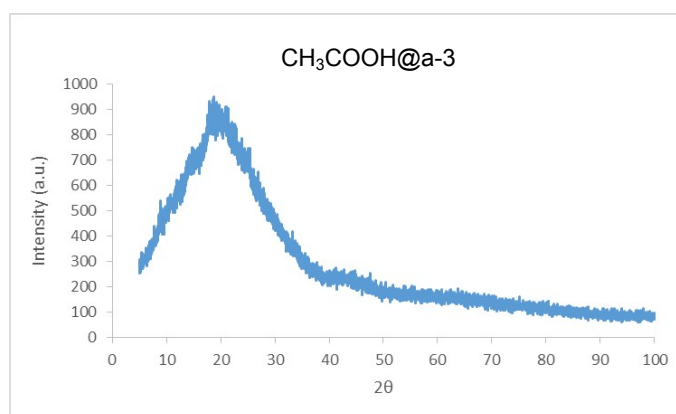


Figure S1. PXRD diffractogram for **CH₃COOH@a-3**

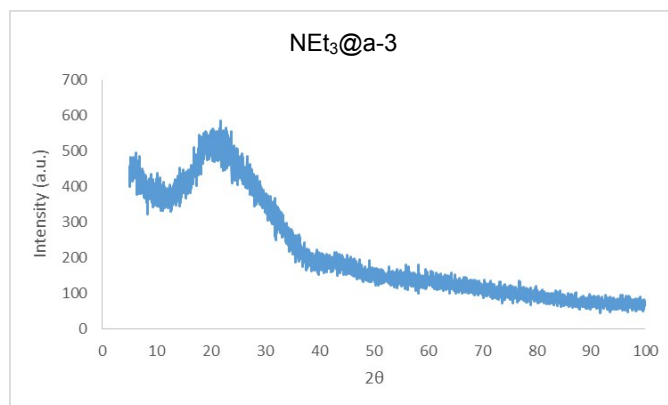


Figure S2. PXRD diffractogram for **Et₃N@a-3**

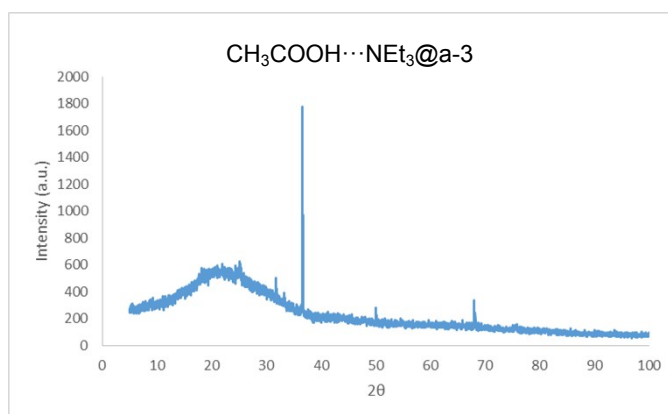


Figure S3. PXRD diffractogram for **CH₃COOH·Et₃N@a-3**

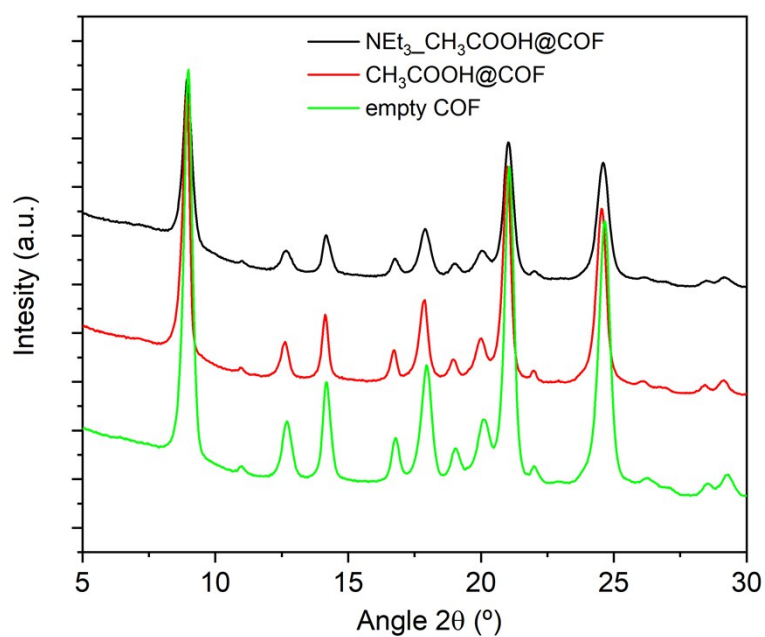


Figure S4. PXRD diffractogram c-3 materials

3. SEM images for a-3 materials

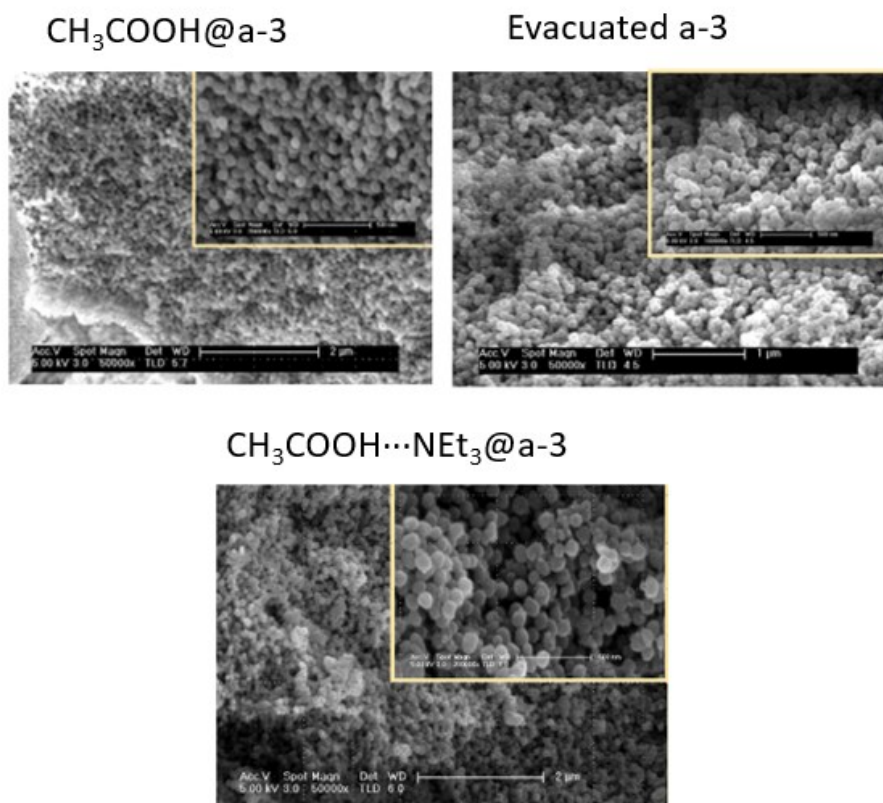


Figure S5. SEM images for a-3 materials

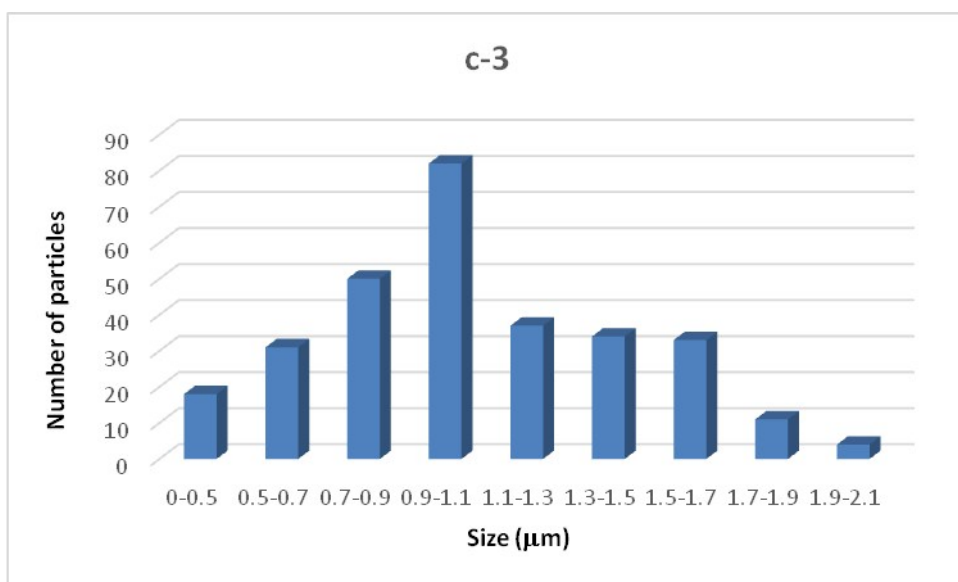
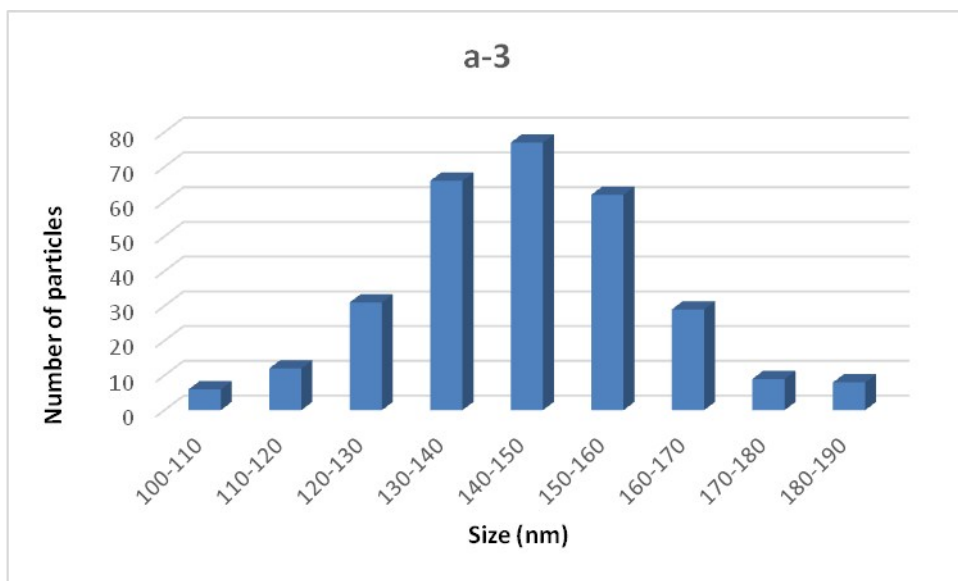


Figure S6. Particle Size Distribution for **a-3** and **c-3** materials

4. NMR-Spectra of the materials

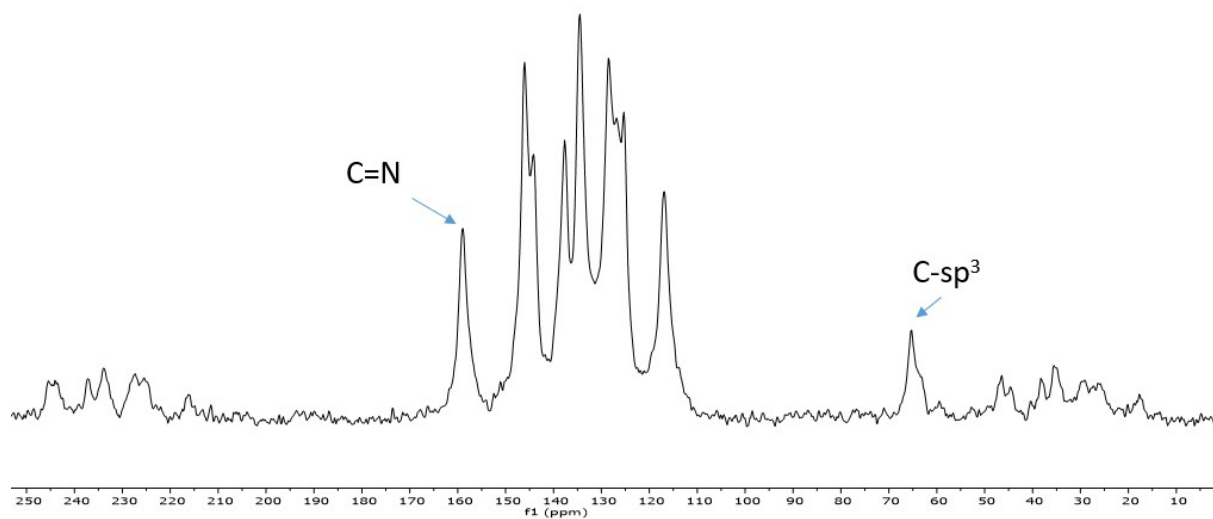
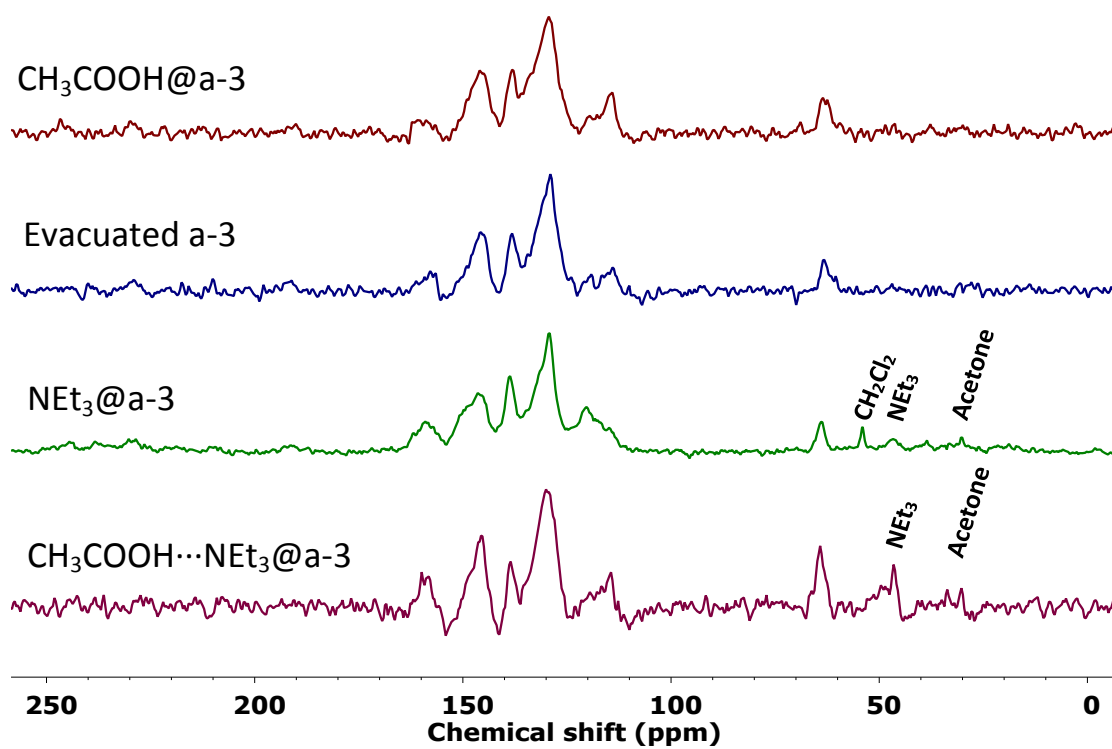


Figure S7. MAS-¹³C NMR for for **a-3** and **c-3** materials

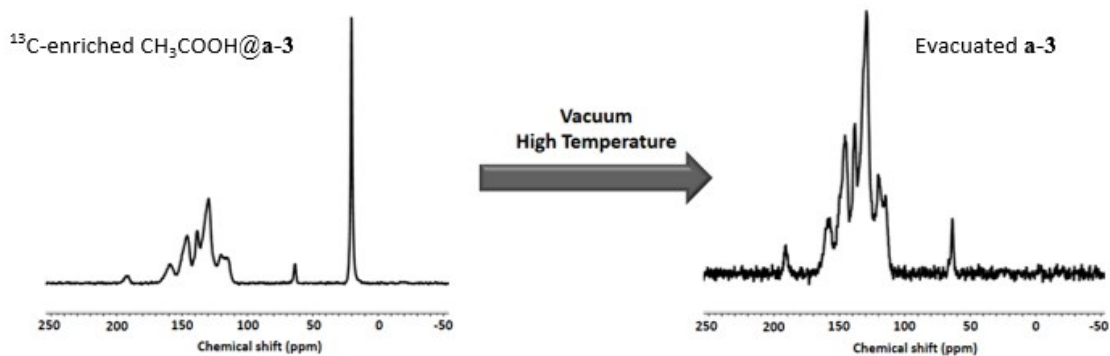


Figure S8. MAS- ^{13}C solid NMR for $\text{CH}_3\text{COOH}@a-3$ containing ^{13}C -enriched acetic acid. Characteristic signal of acetic acid (20 ppm) disappears after treatment of the sample under vacuum at high temperature.

5. IR spectra

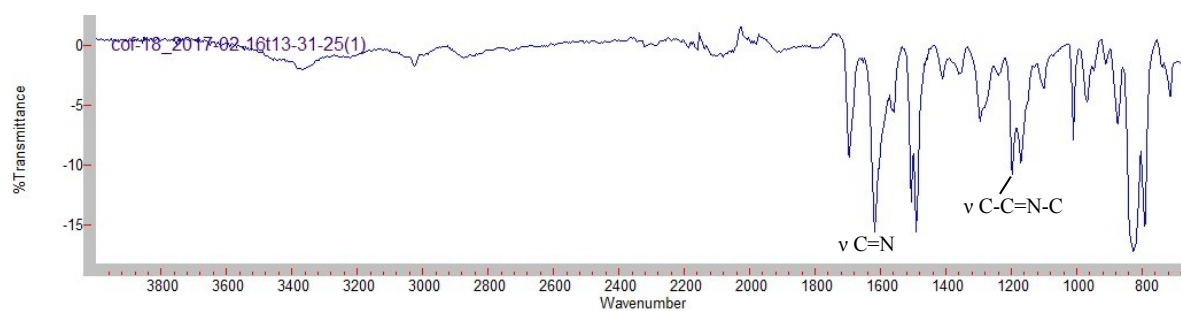


Figure S9. IR spectra for $\text{CH}_3\text{COOH}@a-3$

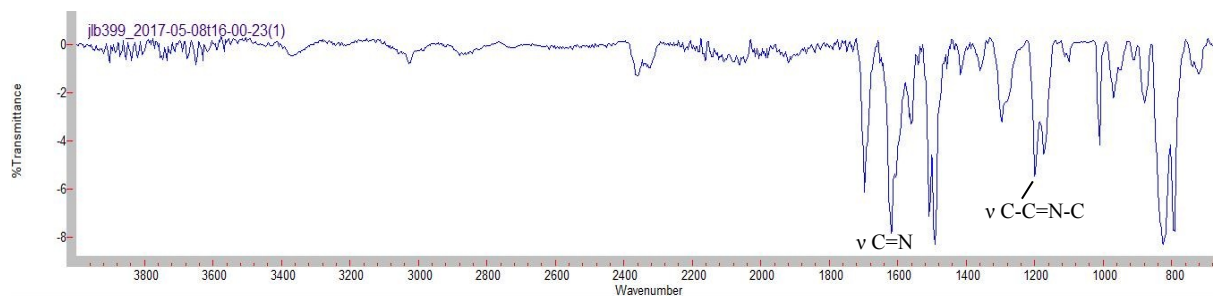


Figure S10. IR spectra for **Evacuated a-3**

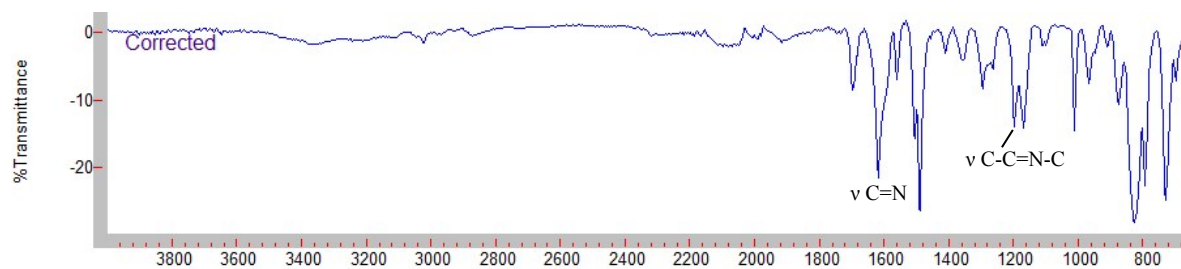


Figure S11. IR spectra for $\text{Et}_3\text{N}@a-3$

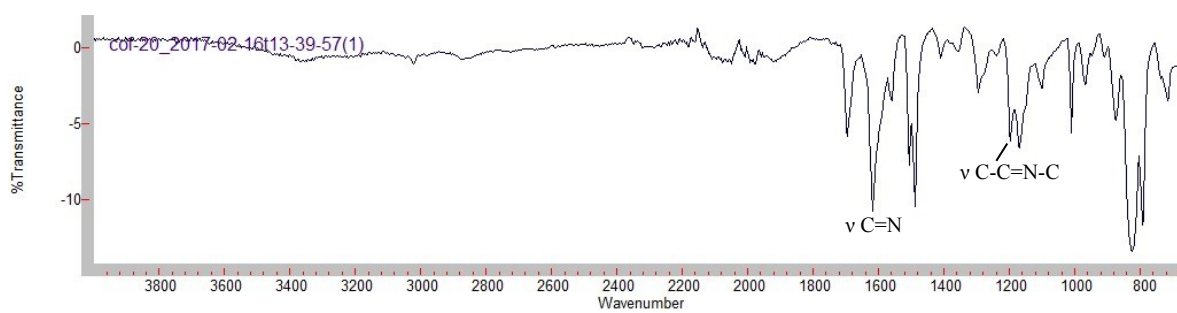


Figure S12. IR spectra for $\text{CH}_3\text{COOH} \cdot \text{Et}_3\text{N} @ \mathbf{a-3}$

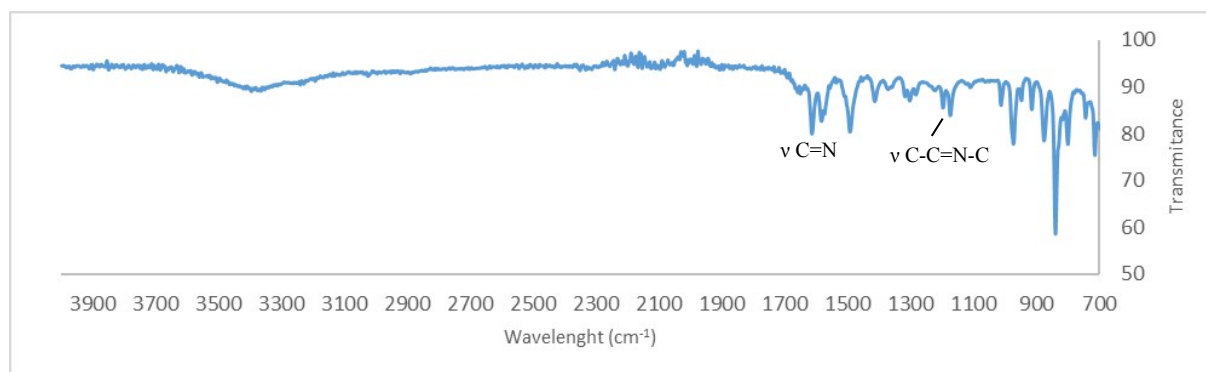
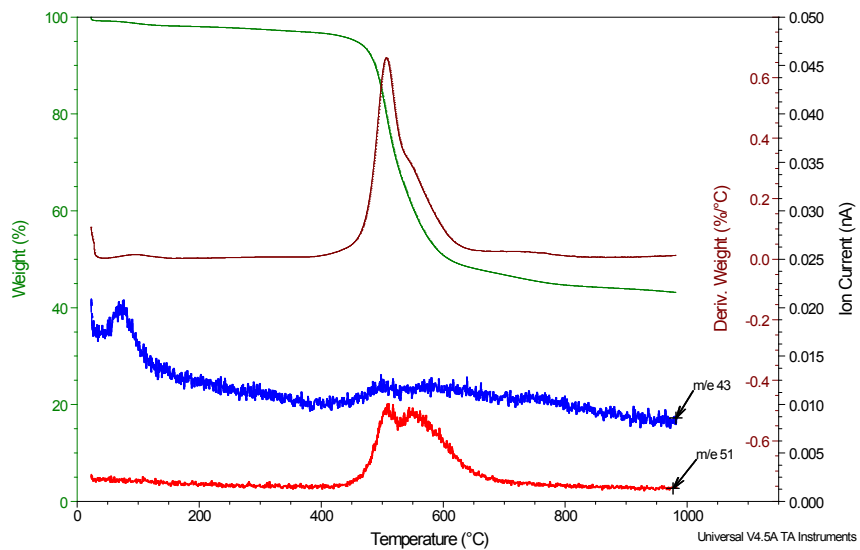


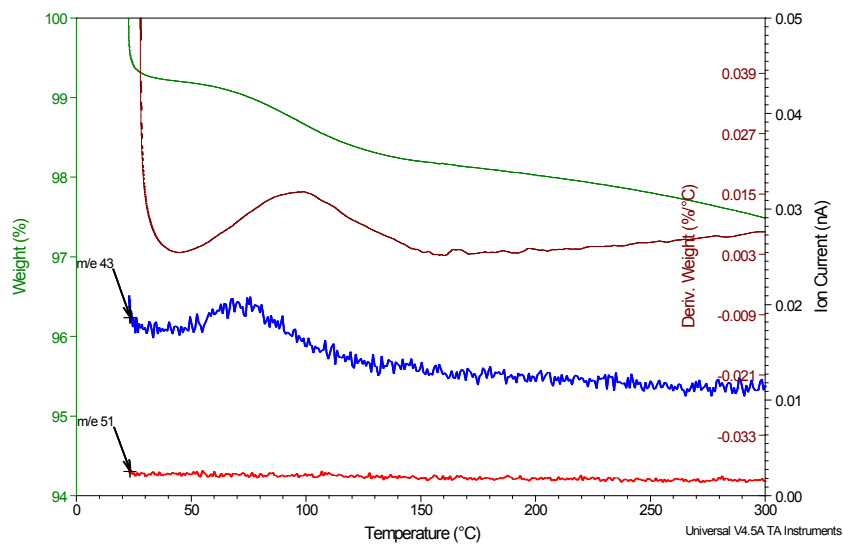
Figure S13. IR spectra for Evacuated $\mathbf{c-3}$

6. TGA-MS

CH₃COOH@COF



CH₃COOH@COF



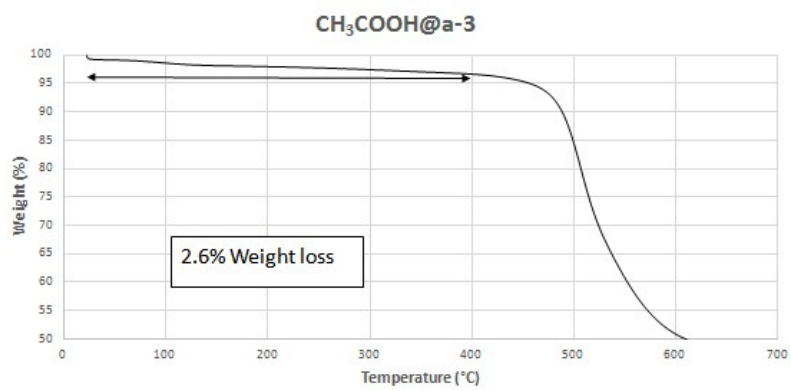
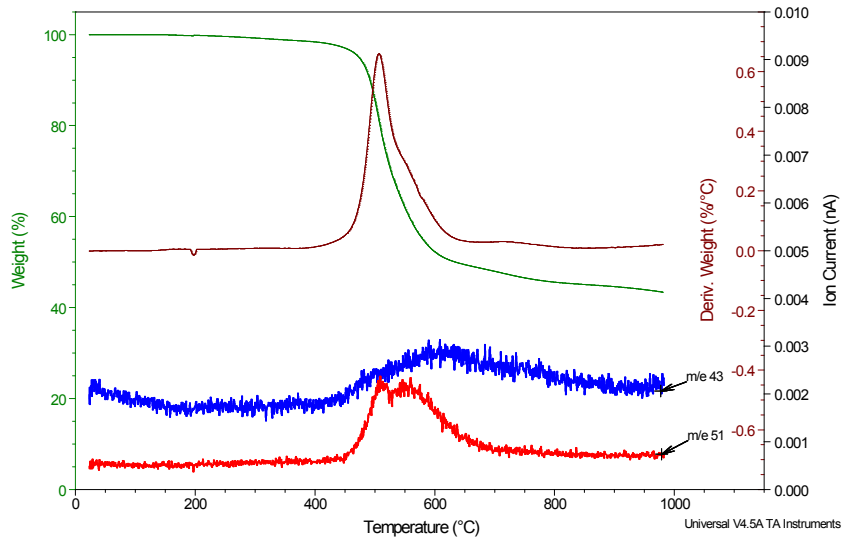
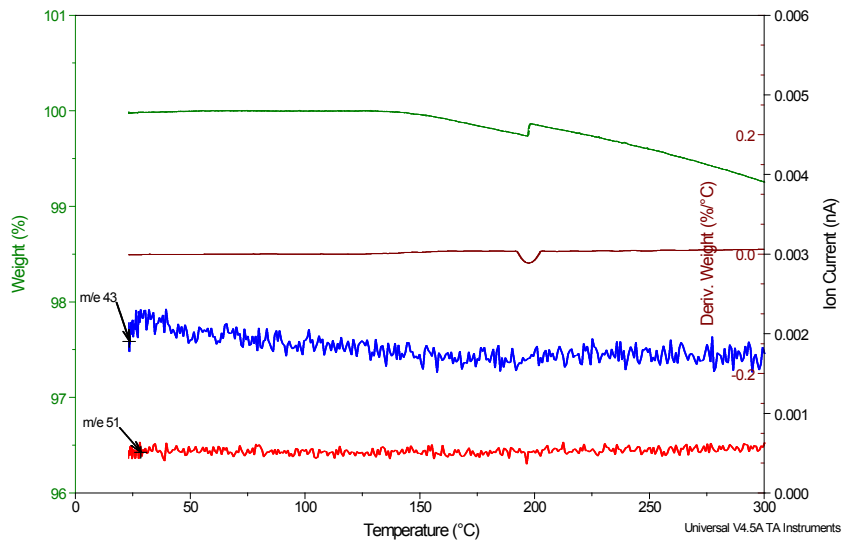


Figure S14. TGA-MS spectra for **CH₃COOH@a-3**

Empty COF



Empty COF



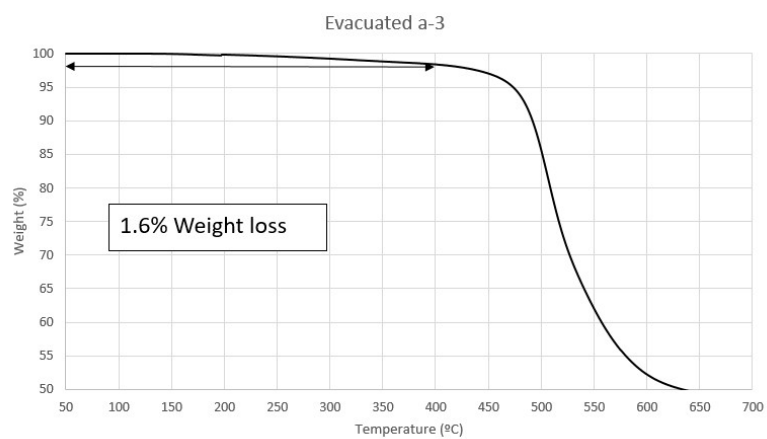


Figure S15. TGA-MS spectra for **Evacuated a-3**

NEt₃@a-3

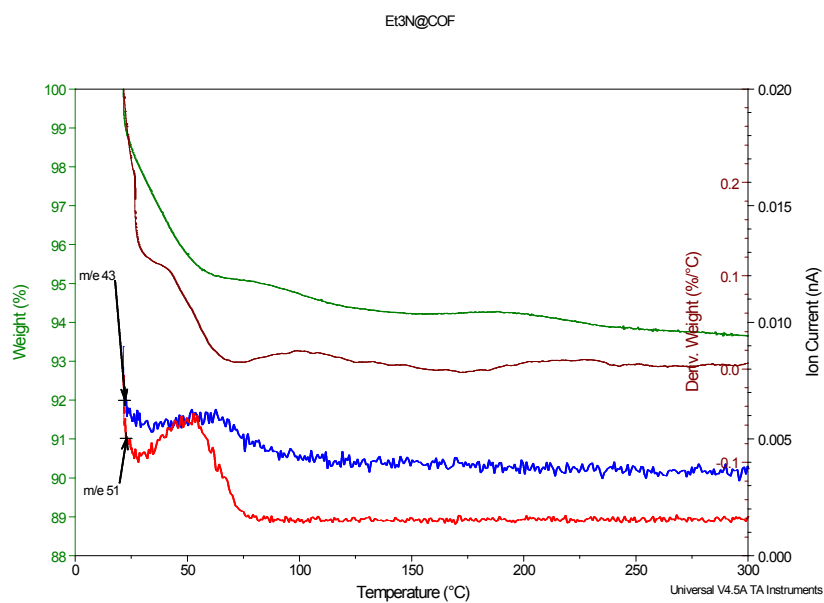
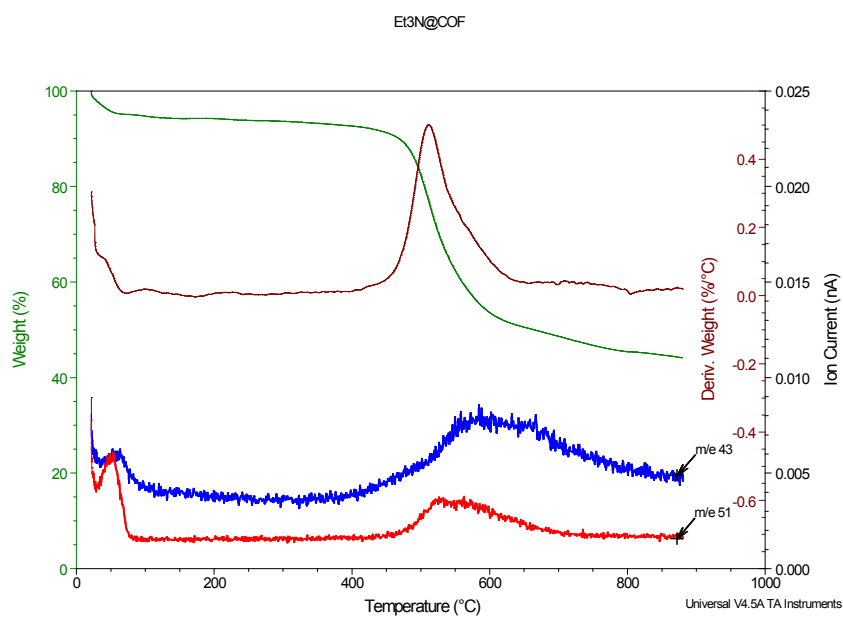
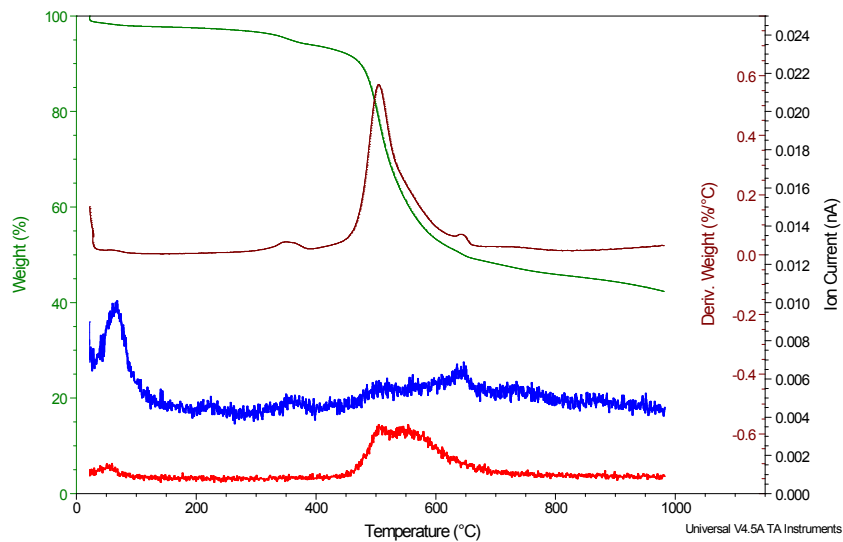


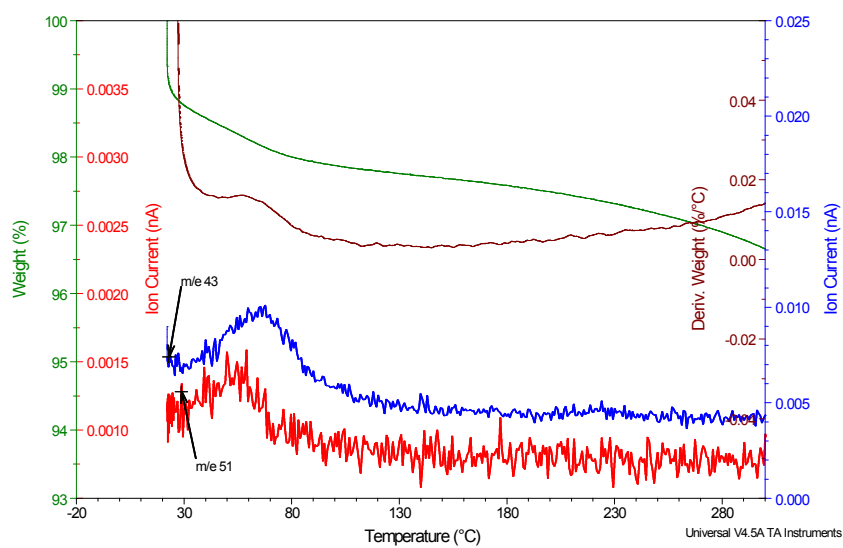
Figure S16. TGA-MS spectra for Et₃N@a-3

CH₃COOH···NEt₃@a-3

CH₃COOH···NEt₃@COF



CH₃COOH···NEt₃@COF



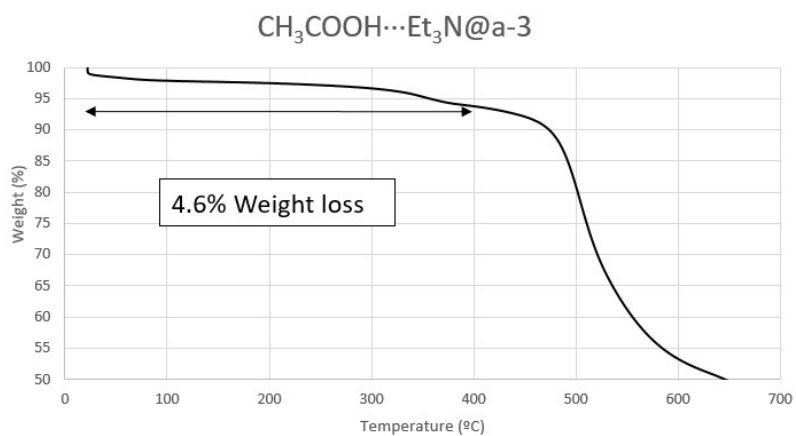


Figure S17. TGA-MS spectra for $\text{CH}_3\text{COOH}\cdots\text{Et}_3\text{N@a-3}$

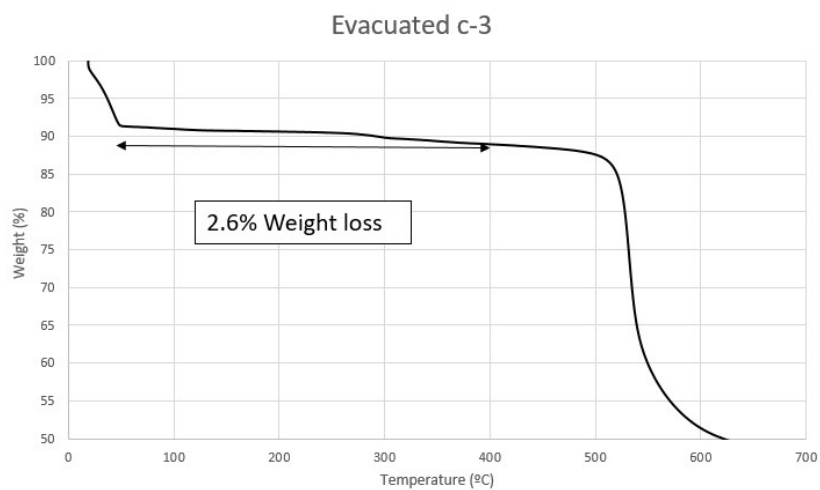


Figure S18. TGA-MS spectra for **Evacuated c-3**

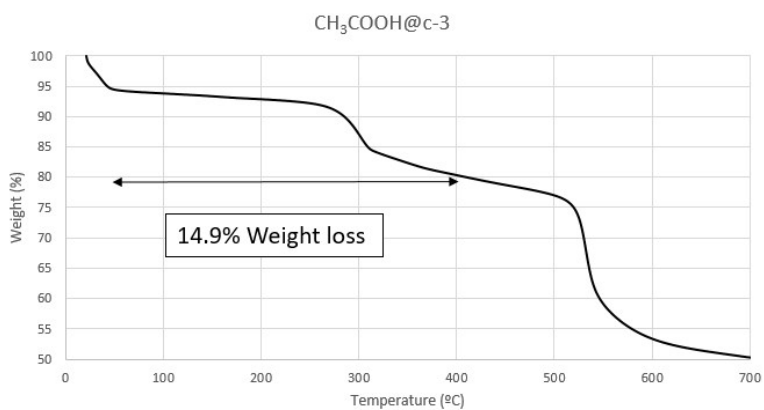


Figure S19. TGA-MS spectra for $\text{CH}_3\text{COOH@c-3}$

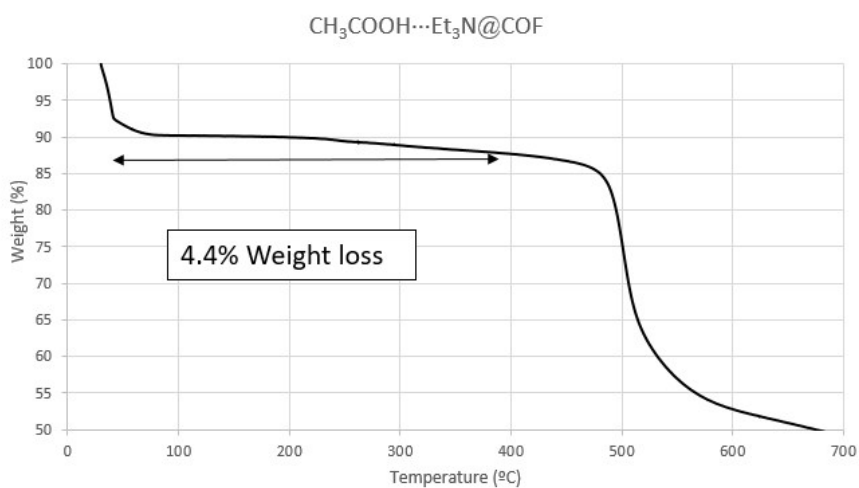
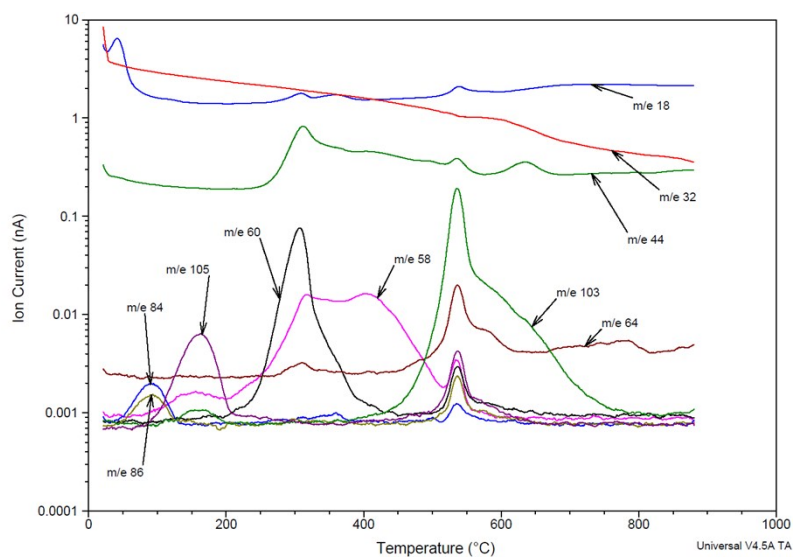
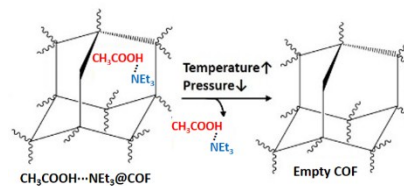


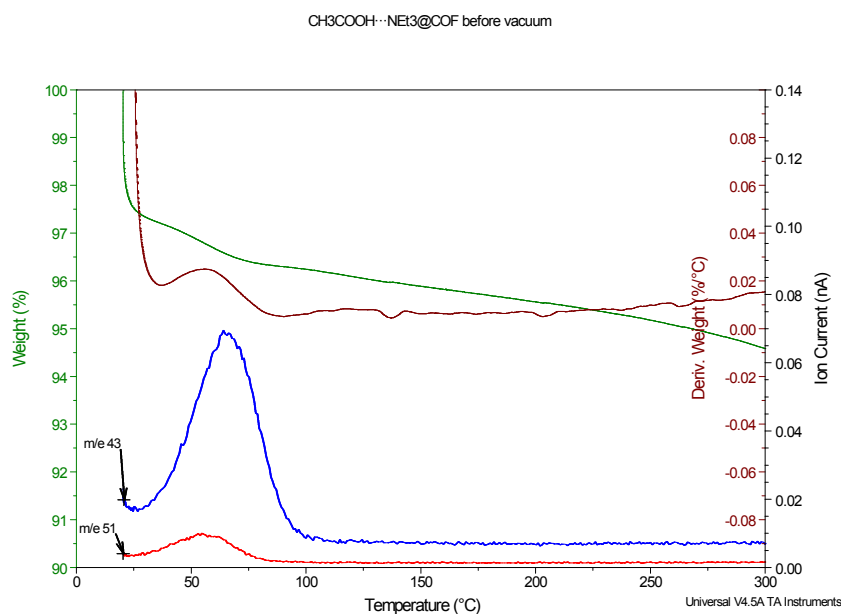
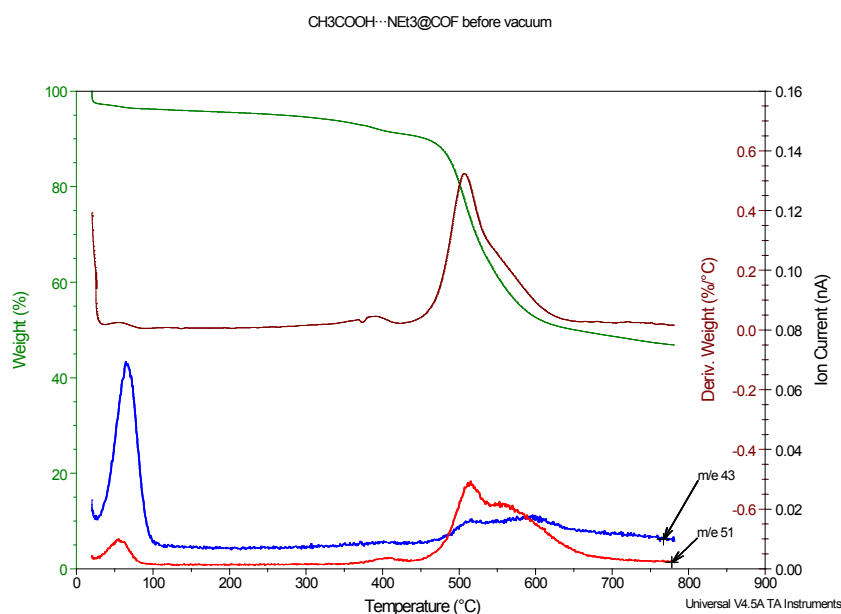
Figure S20. TGA-MS spectra for $\text{CH}_3\text{COOH}\cdots\text{Et}_3\text{N@c-3}$

Switching off the $\text{CH}_3\text{COOH}\cdots\text{NEt}_3@a-3$

In order to demonstrate that the switching of the $\text{CH}_3\text{COOH}\cdots\text{NEt}_3@a-3$ can be done in any direction, a sample of this material was synthesized and the TGA-MS was measured. Then, the material was transferred to a 10 mL flask and vacuum was applied during twelve hours while the flask is in a bath at 80°C . A new TGA-MS analysis was done. Comparing both TGA, it can be confirmed that the material lost the $\text{CH}_3\text{COOH}\cdots\text{NEt}_3$, becoming “Empty COF”



Before Vacuum:



After Vacuum:

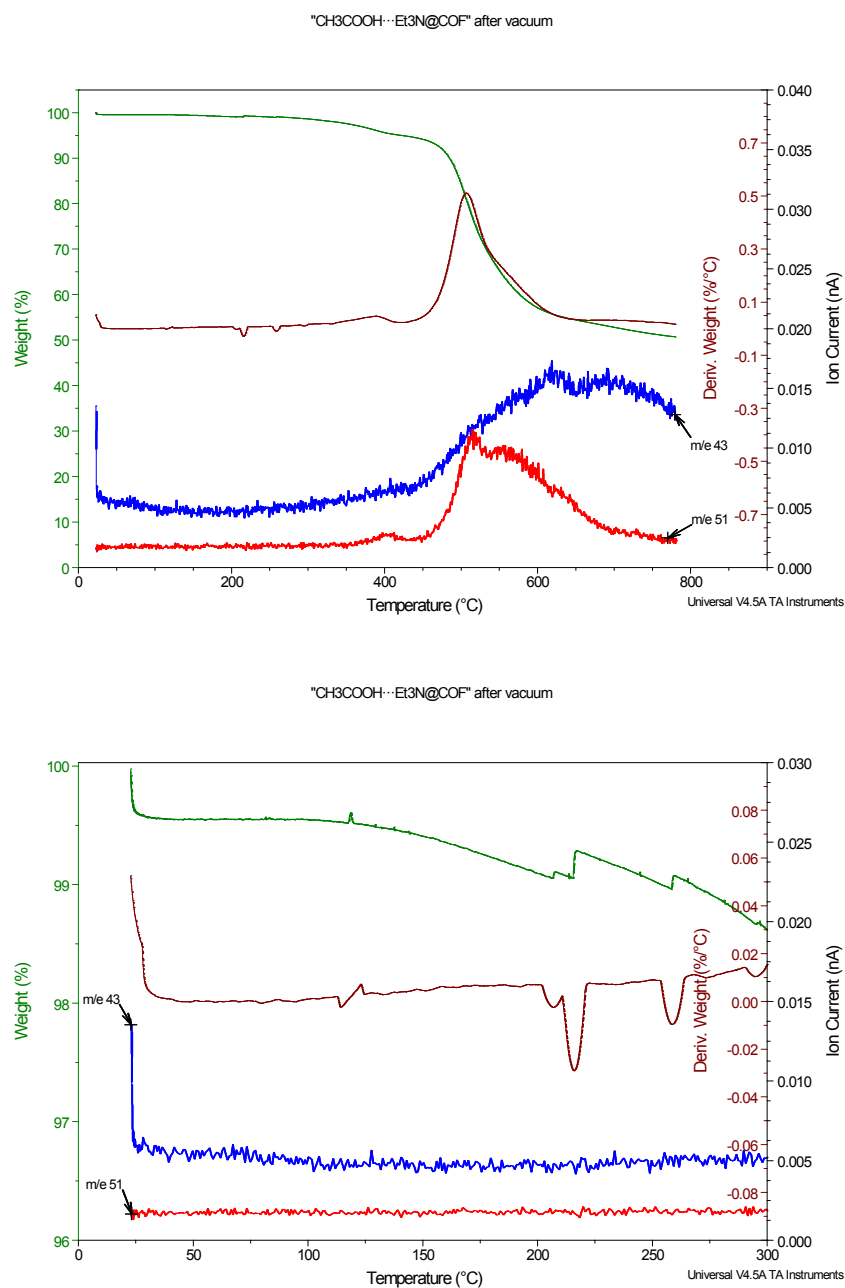
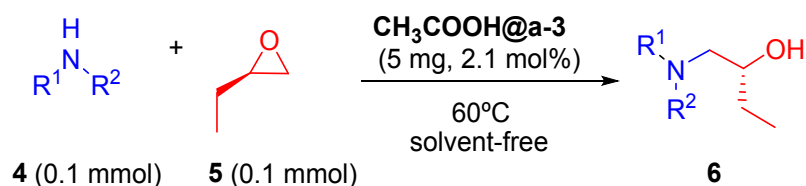


Figure S21. TGA-MS spectra for CH₃COOH···Et₃N@a-3 before and after vacuum

7. General procedure for the catalysis with the amorphous materials and characterization of products

All the catalytic experiments reported below were performed during a two weeks period from the synthesis of material, because we observed that storage of the materials for longer periods results in the decrease of catalytic activity, probably due to loss CH_3COOH and/or NEt_3 volatile molecules.

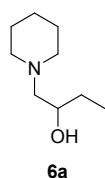
7.1 Epoxide opening catalyzed by $\text{CH}_3\text{COOH}@a-3$



A screw cap with PTFE liner vial was charged with 0.1 mmol of the corresponding amine **4**, 0.1 mmol of the epoxide **5** and 5 mg of the $\text{CH}_3\text{COOH}@a-3$. The vial was warmed to 60°C during the corresponding time (see **Schemes 2** and **3** in the main text). To check the conversion, 1 mL of toluene is added to the vial. Then, an aliquot of 200 μL is taken and 500 μL of a 0.005 M solution of 2-methylnaphthalene (the standard for GC) in toluene was added to the aliquot. The aliquot is analyzed by gas chromatography with a flame ionization detector (FID).

The products of the reaction were previously synthesized using a reported procedure¹, in order to identify the retention time in the gas chromatography – FID and to make a calibration for quantitative analysis.

1-(Piperidin-1-yl)butan-2-ol (**6a**)

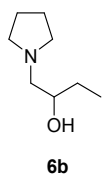


¹H-NMR (300 MHz, CDCl_3): δ 3.74 (bs, 1H), 3.57 (dddd, $J = 10.3, 7.0, 5.2, 3.3$ Hz, 1H), 2.69-2.46 (m, 2H), 2.29 (dd, $J = 12.2, 3.3$ Hz, 1H), 2.28 – 2.22 (m, 2H), 2.16 (dd, $J = 12.2, 10.5$ Hz, 1H), 1.69 – 1.50 (m, 4H), 1.50 – 1.31 (m, 4H), 0.96 (t, $J = 7.5$ Hz, 3H). The product matched with the previous spectroscopic data described in the literature.^{1,2}

¹ N. Azizi, M. R. Saidi, *Org. Lett.* **2005**, *7*, 3649-3651.

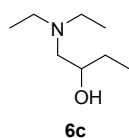
² S. R. Roy, A. Nijamudheen, A. Pariyar, A. Ghosh, P. K. Vardhanapu, P. K. Mandal, A. Datta, S. K. Mandal, *ACS Catal.* **2014**, *4*, 4307-4319.

1-(Pyrrolidin-1-yl)butan-2-ol (6b)



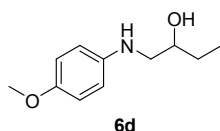
¹H-NMR (300 MHz, CDCl₃): δ 3.64 – 3.49 (m, 1H), 3.48 (s, 1H), 2.72 – 2.63 (m, 2H), 2.56 (dd, *J* = 11.8, 10.7 Hz, 1H), 2.49 – 2.39 (m, 2H), 2.27 (dd, *J* = 11.9, 3.0 Hz, 1H), 1.80 – 1.74 (m, 4H), 1.53 – 1.38 (m, 2H), 0.97 (t, *J* = 7.5 Hz, 3H). The product matched with the previous spectroscopic data described in the literature.¹

1-(Diethylamino)butan-2-ol (6c)



¹H-NMR (300 MHz, CDCl₃): δ 3.50 (dddd, *J* = 10.4, 7.0, 5.2, 3.2 Hz, 1H), 2.64 (dq, *J* = 13.0, 7.3 Hz, 2H), 2.47 (dq, *J* = 13.0, 7.0 Hz, 2H), 2.42 (dd, *J* = 12.6, 3.2 Hz, 1H), 2.22 (dd, *J* = 12.6, 10.5 Hz, 1H), 1.52 – 1.36 (m, 2H), 1.02 (t, *J* = 7.1 Hz, 6H), 0.98 (t, *J* = 7.5 Hz, 3H). The product matched with the previous spectroscopic data described in the literature.³

1-((4-Methoxyphenyl)amino)butan-2-ol (6d)

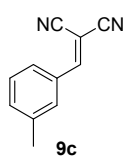


¹H-NMR (300 MHz, CDCl₃): δ 6.84 – 6.75 (m, 2H), 6.68 – 6.59 (m, 2H), 3.81 – 3.68 (m, 1H), 3.75 (s, 3H), 3.22 (dd, *J* = 12.6, 3.1 Hz, 1H), 2.95 (dd, *J* = 12.6, 8.6 Hz, 1H), 1.65 – 1.48 (m, 2H), 1.01 (t, *J* = 7.5 Hz, 3H). The product matched with the previous spectroscopic data described in the literature.⁴

³ S. J. Stropoli, M. J. Elrod, *J. Phys. Chem. A* **2015**, *119*, 10181–10189.

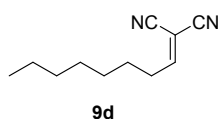
⁴ P. C. Miller, T. J. Owen, J. M. Molyneaux, J. M. Curtis, C. R. Jones, *J. Comb. Chem.* **1999**, *1*, 223-234.

2-(3-Methylbenzylidene)malononitrile (9c)



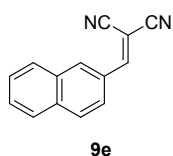
¹H-NMR (300 MHz, CDCl₃): δ 8.14 – 8.06 (m, 2H), 7.54 – 7.46 (m, 1H), 7.41 – 7.30 (m, 2H), 2.45 (s, 3H). The product matched with the previous spectroscopic data described in the literature.⁷

2-Octylidenemalononitrile (9d)



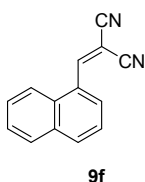
¹H-NMR (300 MHz, CDCl₃): 7.33 (t, *J* = 8.0 Hz, 1H), 2.59 (q, *J* = 7.5 Hz, 2H), 1.56 (quint, *J* = 6.9 Hz, 2H), 1.44 – 1.20 (m, 8H), 0.97 – 0.83 (m, 3H). The product matched with the previous spectroscopic data described in the literature.⁸

2-(Naphthalen-2-ylmethylene)malononitrile (9e)



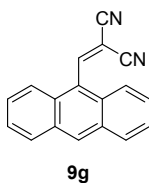
¹H NMR (300 MHz, CDCl₃) δ 8.30 (s, 1H), 8.08 (dd, *J* = 8.7, 1.9 Hz, 1H), 7.96 (d, *J* = 8.5 Hz, 2H), 7.93 – 7.88 (m, 2H), 7.73 – 7.58 (m, 2H). The product matched with the previous spectroscopic data described in the literature.⁶

2-(Naphthalen-1-ylmethylene)malononitrile (9f)



¹H-NMR (300 MHz, CDCl₃): δ 8.66 (s, 1H), 8.28 (d, *J* = 7.3 Hz, 1H), 8.12 (d, *J* = 8.2 Hz, 1H), 7.97 (d, *J* = 7.9 Hz, 2H), 7.75 – 7.57 (m, 3H). The product matched with the previous spectroscopic data described in the literature.⁷

2-(Anthracen-9-ylmethylene)malononitrile (9g)



¹H NMR (300 MHz, CDCl₃): δ 8.97 (s, 1H), 8.66 (s, 1H), 8.15 – 8.07 (m, 2H), 7.98 – 7.90 (m, 2H), 7.73 – 7.65 (m, 2H), 7.63 – 7.55 (m, 2H). The product matched with the previous spectroscopic data described in the literature.⁷

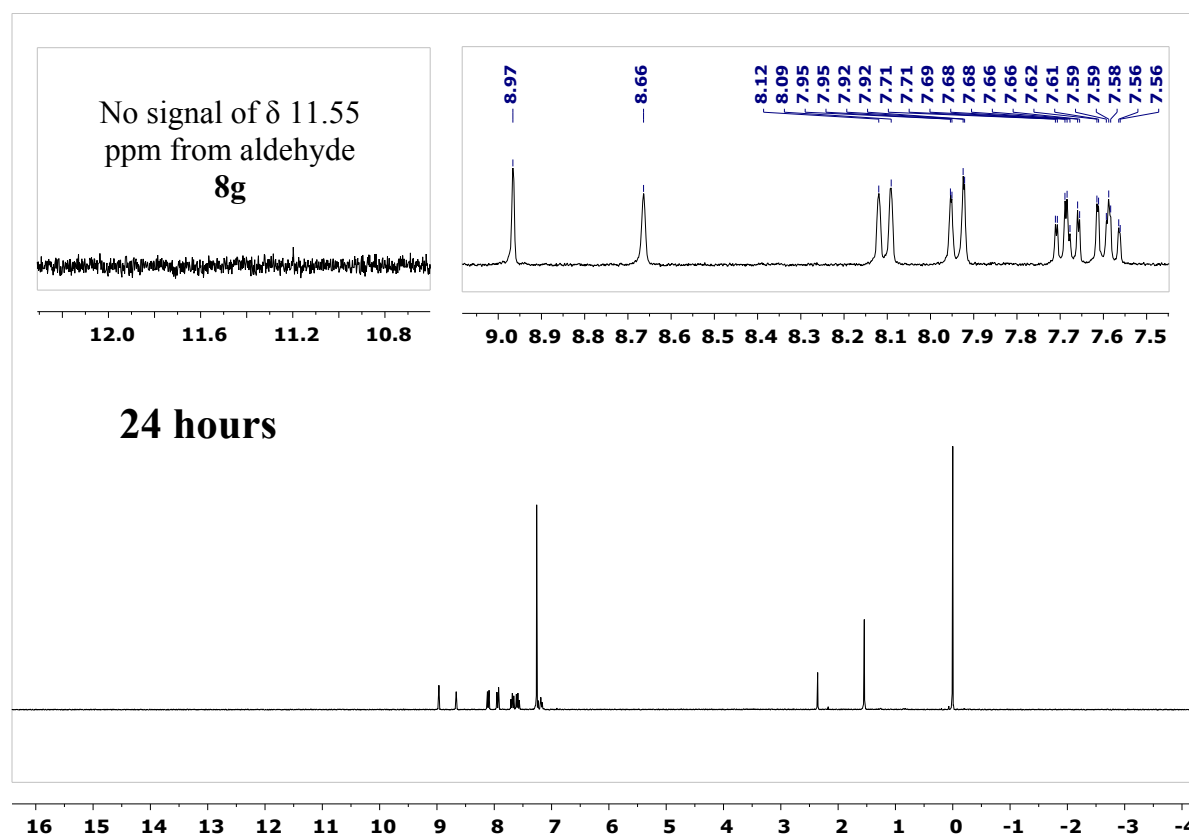
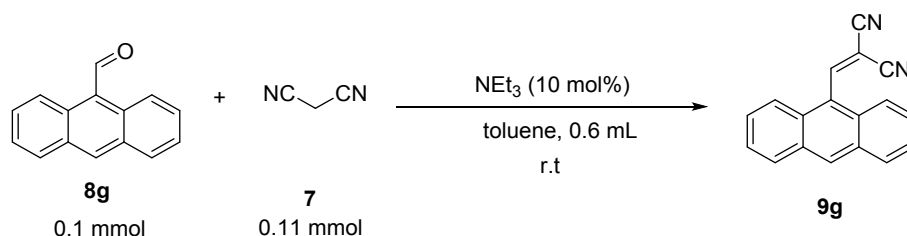
⁷ M.M.H. Bhuiyan, M.I. Hossain, M. Ashraful Alam and M.M. Mahmud, *Chemistry Journal* **2012**, *2*, 31-37.

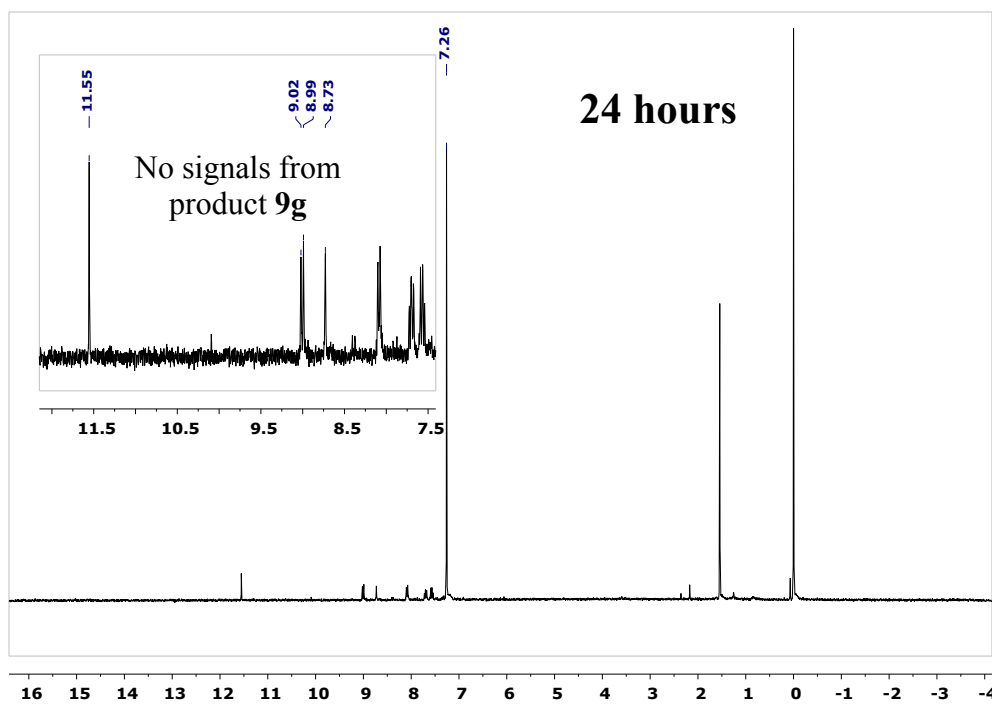
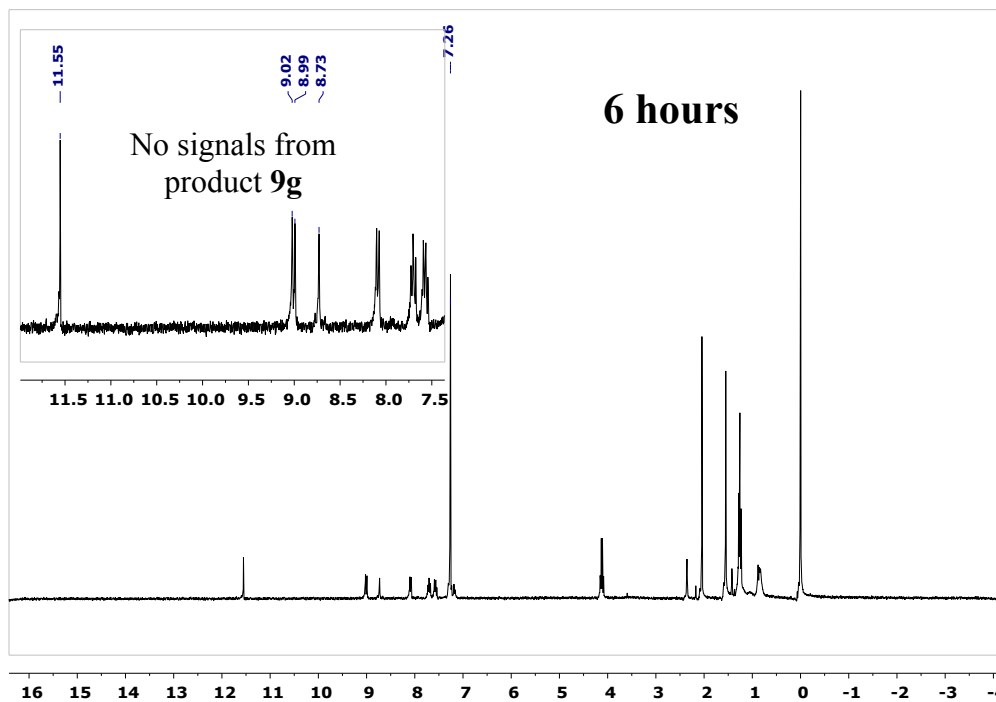
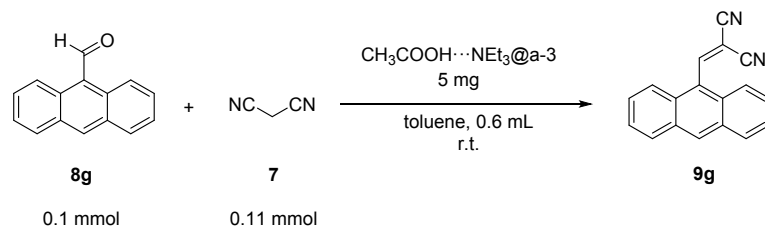
⁸ Y. Jia, Y. Fang, Y. Zhang, H. N. Miras, Y.-F. Song, *Chem. Eur. J.* **2015**, *21*, 14862 –1487.

7.3 Formation of 9g catalyzed by COF and by NEt₃

Anthracene-9-carbaldehyde **8g** and 2-(anthracen-9-ylmethylene)malononitrile **9g** are not volatile enough to analyze them by Gas Chromatography (GC) so the conversion of this reaction was determined by ¹H-NMR spectrum of the reaction mixture. The reactions were set up following the general conditions for the catalyzed Knoevenagel condensation using the corresponding catalyst. At the indicated time, an aliquot of 100 μL was taken, the solvent was removed in the rotavap and it was analyzed by ¹H-NMR using CDCl₃ as solvent.

This reaction reached the 100 % of conversion with free triethylamine, indicating that the reaction can be catalyzed in basic conditions. However, using CH₃COOH⋯NEt₃@**a-3** as catalyst, no formation of the product was observed (see ¹H-NMR spectra below) suggesting a size-selectivity in the pores of the COF.

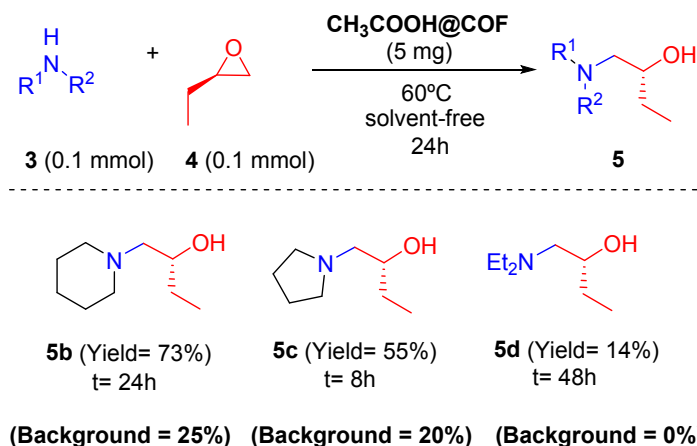




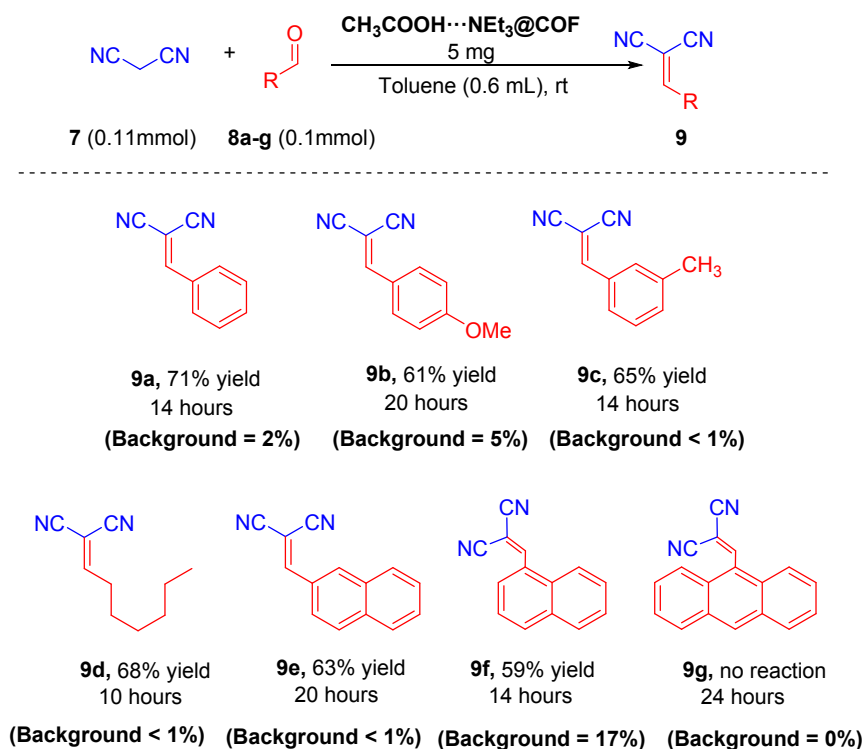
7.4 Epoxide opening and Knoevenagel background reactions

In order to verify that the reactions were catalyzed by the $\text{CH}_3\text{COOH}@a-3$ or the $\text{CH}_3\text{COOH}\cdots\text{NEt}_3@a-3$, we always carried out all the reactions in the general conditions but without using a catalyst (Background reactions). In the next two tables the background yield of each reaction is shown to compare with the yield of the catalyzed reaction (both yields for the same time reaction).

Epoxide Opening:



Knoevenagel condensation:



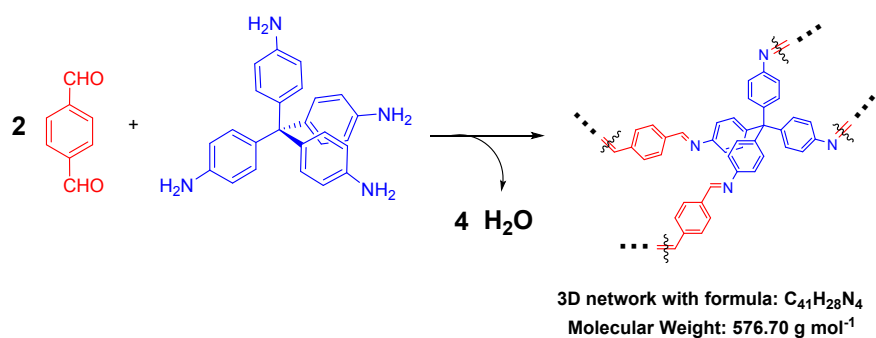
8. Calculation of chemical erosion of COF

Some representative reactions of the Epoxide Opening or the Knoevenagel condensation were carried out following the general conditions but using only one of the two reagents, in order to check if the reagent reacts with the COF and to recognize possible byproducts.

In the case of the experiments carried out with the general conditions for the “Epoxide Opening”, at the indicated time, CDCl_3 was directly added to the reaction mixture. Then the solution was analyzed by $^1\text{H-NMR}$.

In the case of the experiments carried out with the general conditions for the “Knoevenagel condensation”, at the indicated time, an aliquot of 100 μL was taken, the solvent was removed in the rotavap and it was analyzed by $^1\text{H-NMR}$ (CDCl_3). The reaction using both **8a** and **7** was also analyzed in this manner.

To calculate the amount of deteriorated COF is necessary to consider the amount of imine functional groups per 5 mg of material:

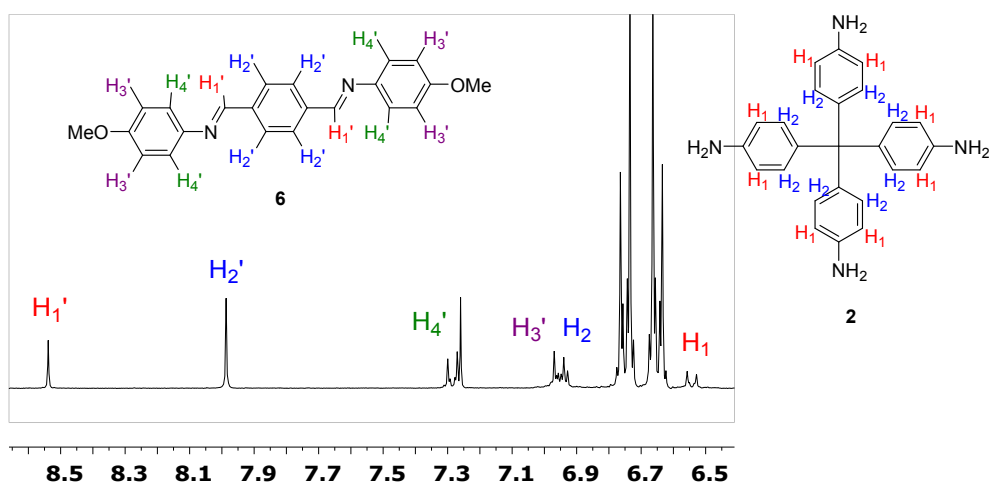
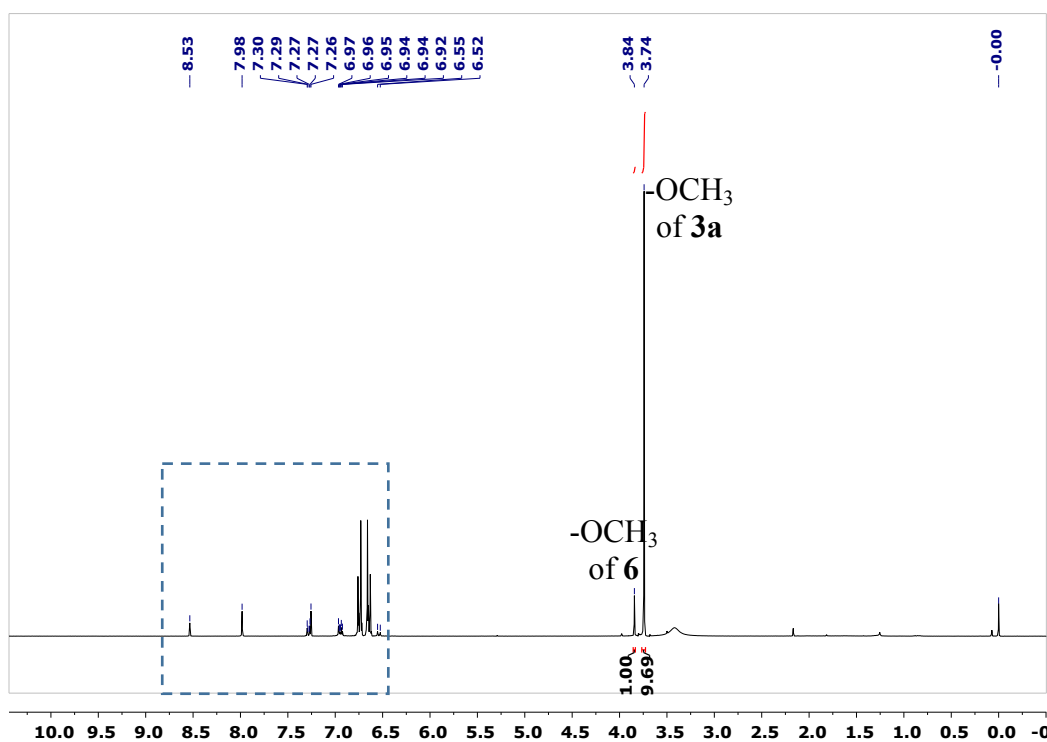
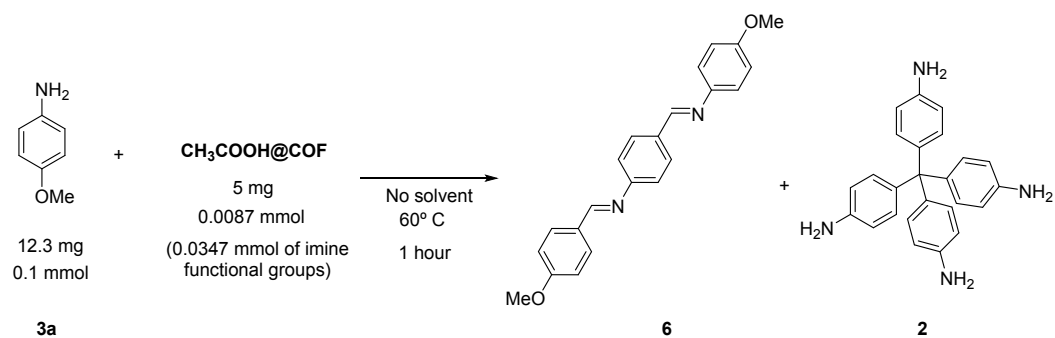


$$5 \text{ mg} / 576.70 \text{ g mol}^{-1} = 0.00867 \text{ mmol.}$$

There is four imine functional groups in this subunit:

$$0.00867 \text{ mmol} \cdot 4 = 0.0347 \text{ mmol of imine functional groups in 5 mg of material.}$$

Calculation of chemical erosion COF with Methoxyaniline 3a



The signals of byproduct 6 matched with the previous spectroscopic data described in the literature.⁹

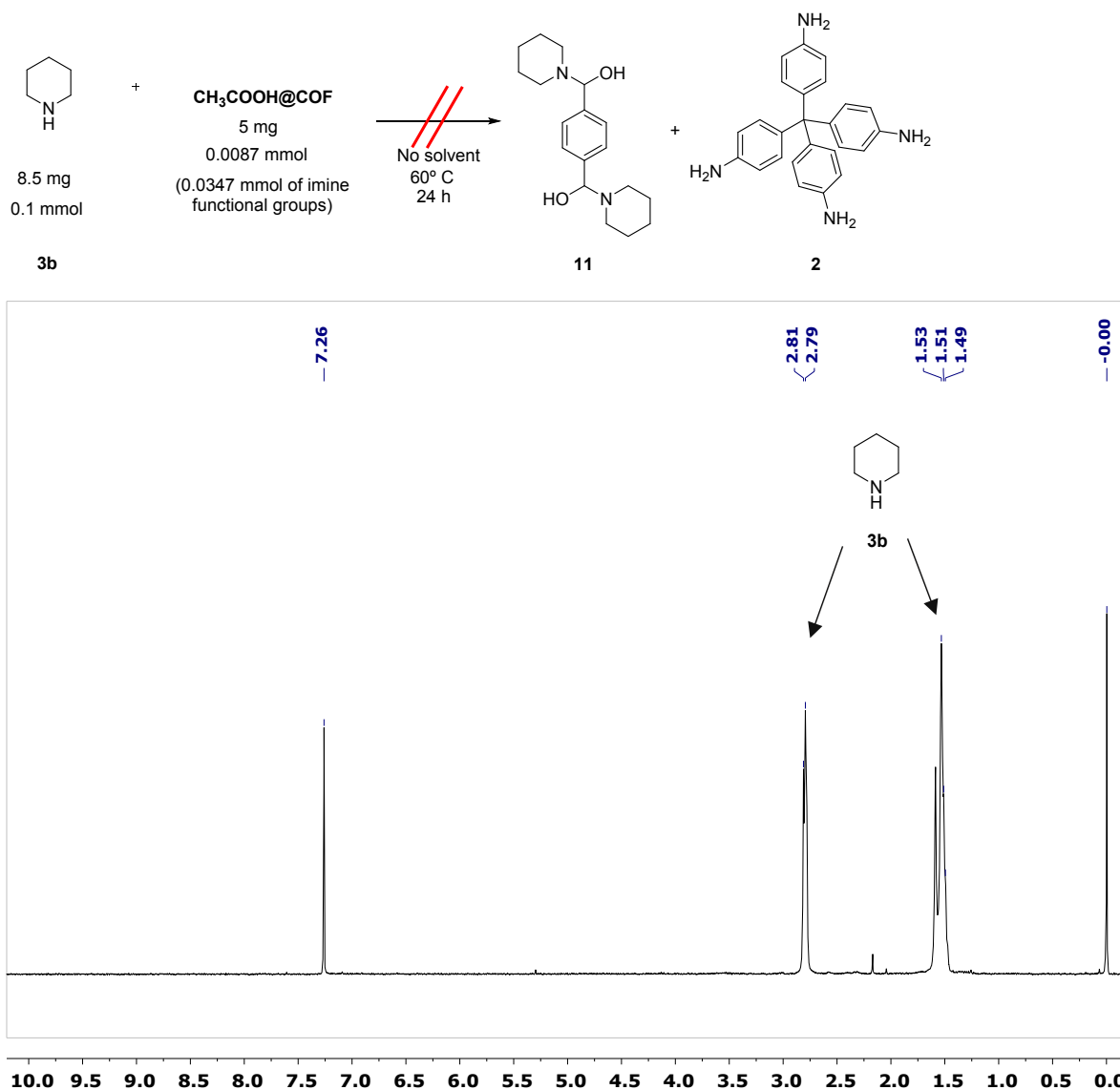
To calculate the ratio (byproduct **6** : methoxyaniline **3a**) we use the signal of 3.84 ppm for byproduct **6** and the signal at 3.74 ppm for methoxyaniline **3a**. The 3.84 ppm signal integrates for six protons, and the 3.74 ppm signal integrates for three protons, so the molar ratio is (0.50 : 9.69).

Considering the stoichiometry, two molecules of methoxyaniline **3a** are necessary for making one molecule of byproduct **6**, so the ratio of (reacted methoxyaniline: methoxyaniline left) is (1.00 : 9.69). In other words, 9.4 % of the initial methoxyaniline has reacted.

In the reaction, there was 0.1 mmol of initial methoxyaniline **3a**. Applying this percentage, 0.0094 mmol of the methoxyaniline has reacted with 0.0094 mmol of the imines functional groups of the COF. Therefore, the percentage of deteriorated COF is:

$$\begin{array}{l} \text{\% chemical erosion COF =} \\ \frac{0.0094 \text{ mmol reacted imines}}{0.0347 \text{ mmol total imines}} \cdot 100 = 27 \% \end{array}$$

Calculation of chemical erosion of COF with piperidine 3b



No byproducts from decomposition of COF were detected.

The signals of byproduct **10** matched with the previous spectroscopic data described in the literature.¹⁰

To calculate the ratio (byproduct **10** : malonitrile **7**) we use the signal of 7.82 ppm for byproduct **10** and the signal at 3.57 ppm for malonitrile **7**. Both signals integrate for 2 protons, so the ratio is (1.00 : 15.82).

Considering the stoichiometry, two molecules of malonitrile **7** are necessary for making one molecule of byproduct **10**, so the ratio of (reacted malonitrile: malonitrile left) is (2.00 : 15.82), in other words, 11.2 % of the initial malonitrile has reacted.

In the reaction, there was 0.11 mmol of initial malonitrile **7**. Applying this percentage, 0.012 mmol of the malonitrile has reacted with 0.012 mmol of the imines functional groups of the COF. Therefore, the percentage of deteriorated COF is:

$$\begin{array}{l} \text{\% chemical erosion of COF =} \\ \frac{0.012 \text{ mmol reacted imines}}{0.0347 \text{ mmol total imines}} \cdot 100 = 35.6 \% \end{array}$$

¹⁰ S. K. Panja, N. Dwivedi, S. Saha, *RSC Adv.* **2015**, *5*, 65526-65531

A crude of the catalyzed reaction with $\text{CH}_3\text{COOH}\cdots\text{NEt}_3\text{@COF}$ was analyzed by $^1\text{H-NMR}$ in order to check the decomposition of the COF in the general conditions. The reaction has finished since the malonitrile (δ 3.57 ppm) has been completely consumed.

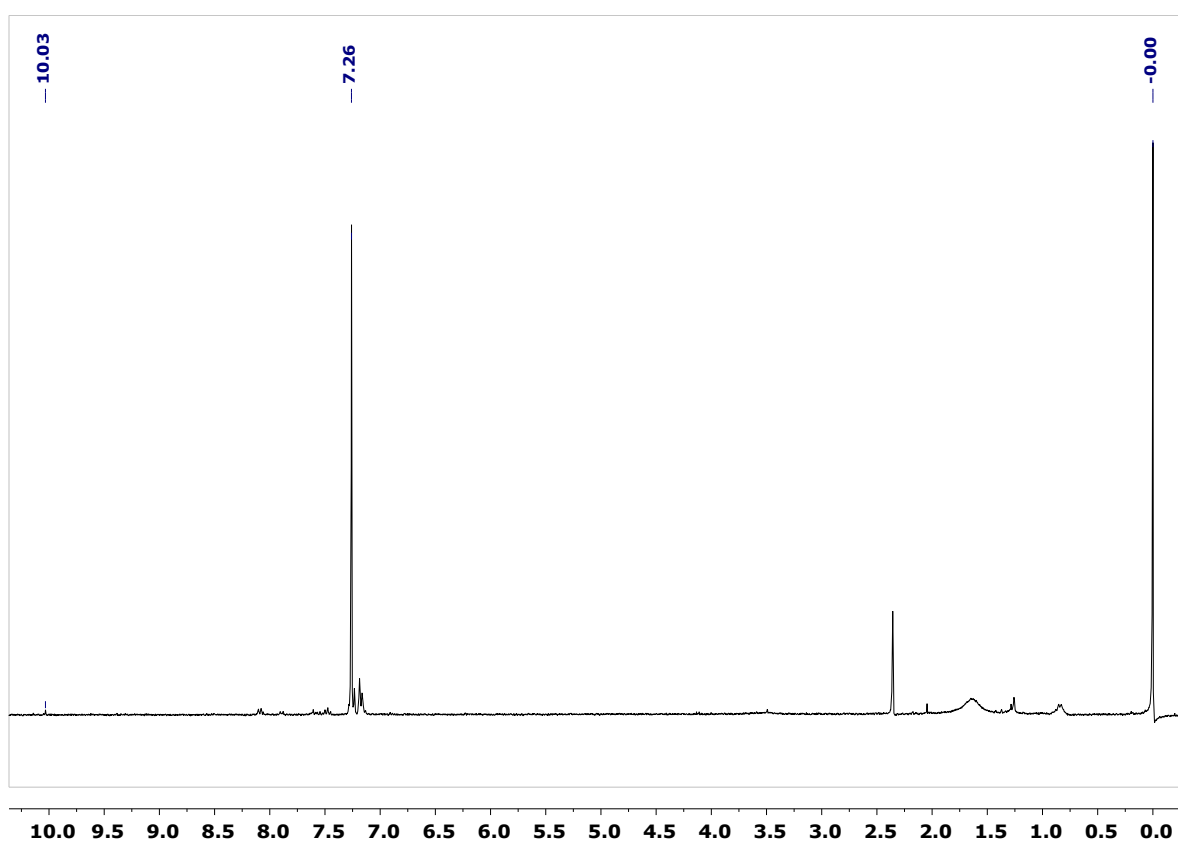
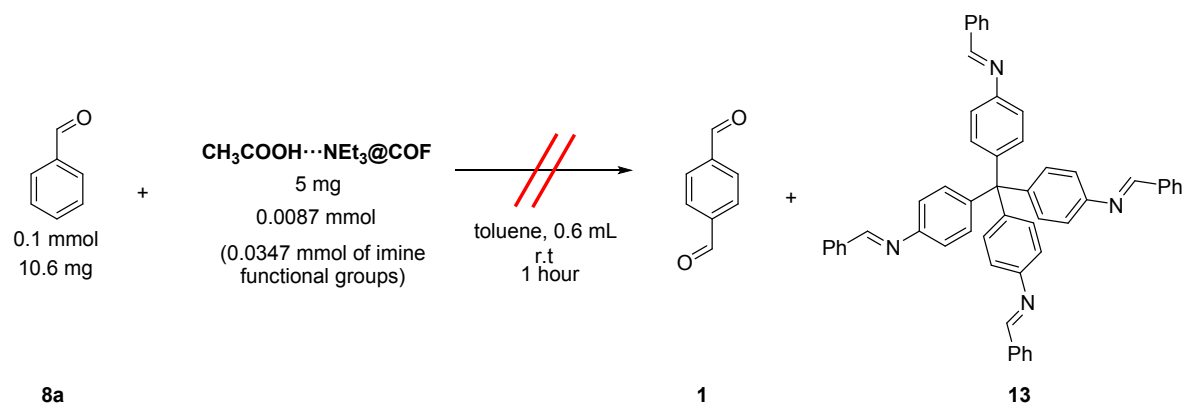
To calculate the ratio (byproduct **10** : product **9a**) we use and the signal at 7.82 ppm for byproduct **10** and the signal at 7.78 ppm for product **9a**. The signal at 7.82 ppm integrates by two protons, and the signal at 7.78 ppm integrates by one proton, so the molar ratio is (0.5 : 22.96).

Considering the stoichiometry, two molecules of malonitrile **7** are necessary for making one molecule of byproduct **10** but only one molecule of malonitrile **7** is necessary for making one molecule of product **9a**. Therefore the ratio of (malonitrile transformed in **10**: malonitrile transformed in **9a**) is (1.00 : 22.69), in other words, 4.2 % of the initial malonitrile has reacted with the COF and 95.8 % of the initial malonitrile has reacted with the benzaldehyde **8a**.

In the reaction, there was 0.11 mmol of initial malonitrile **7**. Applying this percentage, 0.0046 mmol of the malonitrile has reacted with 0.0046 mmol of the imines functional groups of the COF. Therefore, the percentage of deteriorated COF is

$$\begin{array}{l} \text{\% chemical erosion of COF =} \\ \frac{0.0046 \text{ mmol reacted imines}}{0.0347 \text{ mmol total imines}} \cdot 100 = 13.2 \text{ \%} \end{array}$$

Calculation of deteriorated COF with benzaldehyde **8a**

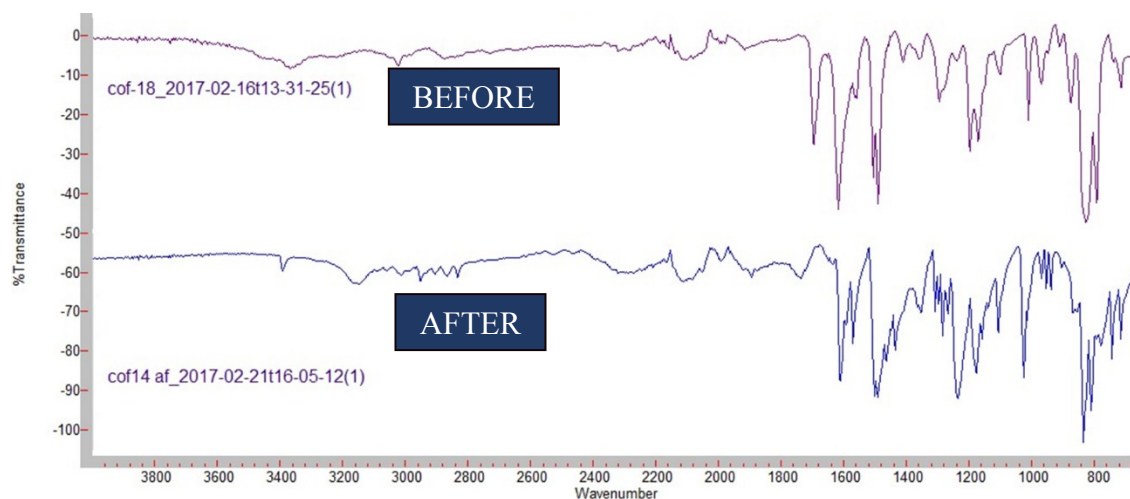
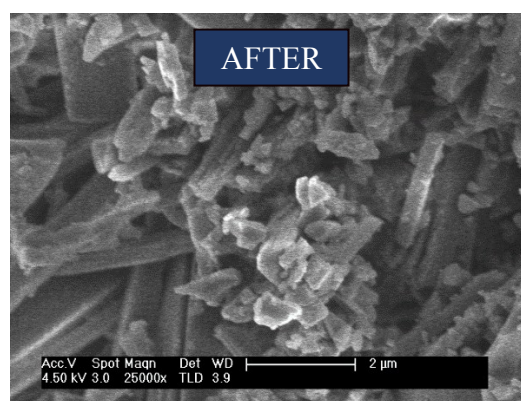
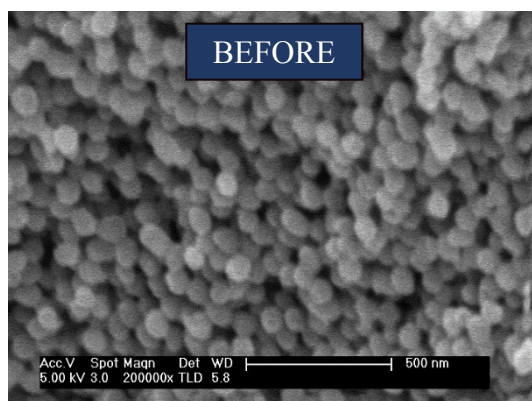
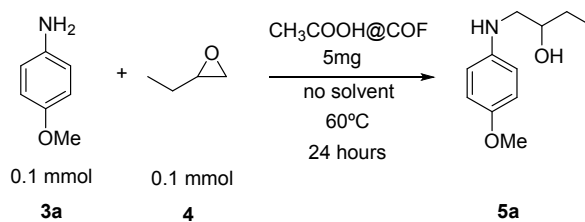


Before carrying out the spectrum, the toluene must be removed in the rotavap. The benzaldehyde **8a**, which is also volatile, is removed too. Some traces of benzaldehyde **8a** and toluene can be hardly seen in the spectrum. However, decomposition products of the COF, like terephthalaldehyde **1**, 4,4',4'',4'''-methanetetrayltetraaniline **2** or byproduct **13** are not volatile and they should be observed in the case they had been formed. Since no traces of these products were found, it can be concluded that the benzaldehyde did not promote the decomposition of the COF.

9. COF stability after reactions

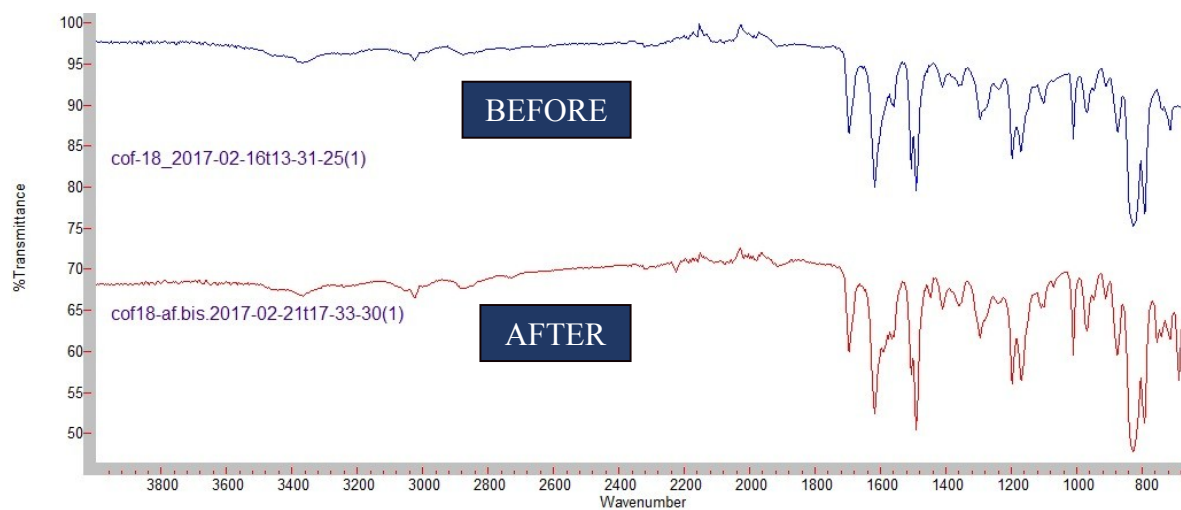
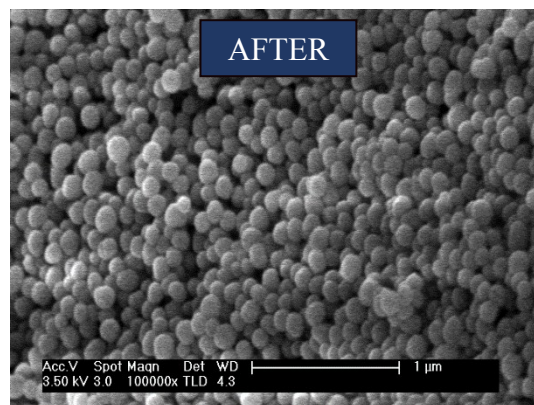
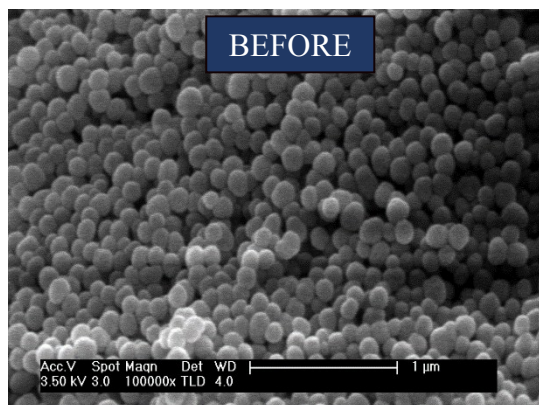
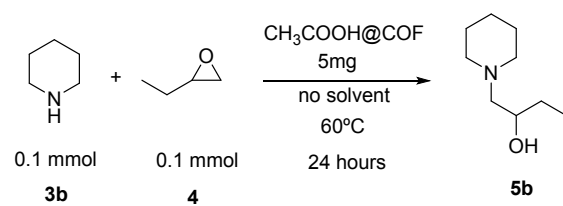
We carried out model reactions using COF as catalyst. After the indicated time, the reaction mixture was passed through a membrane filter of 0.45 μm pores and the solid was washed three times with 10 mL of CH_2Cl_2 .

SEM images and IR spectra were taken from the solid to compare them with the images and spectra of the COF before the reaction.

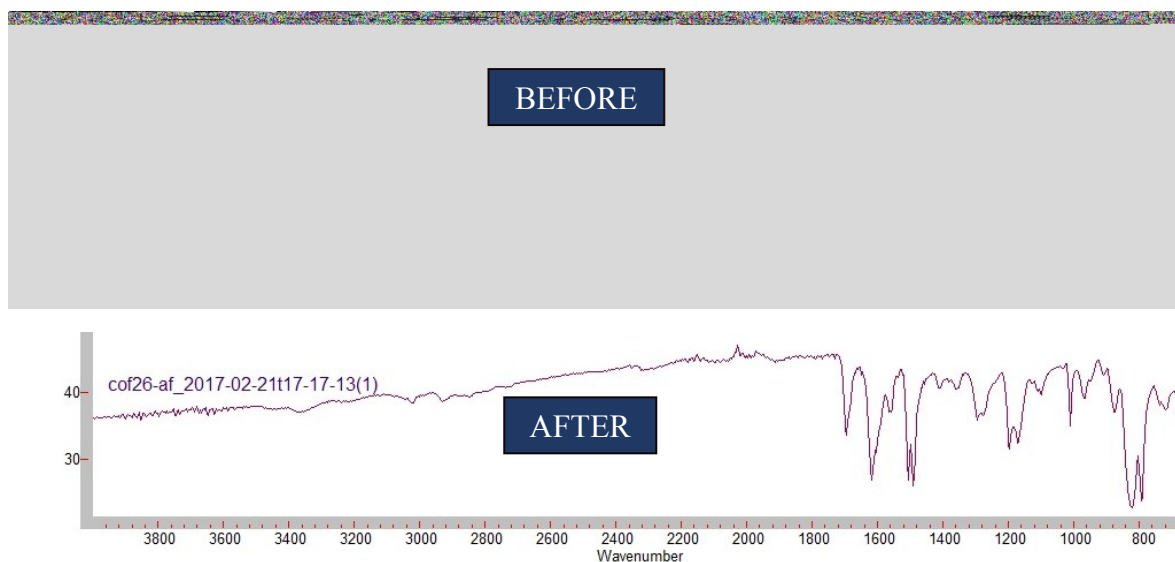
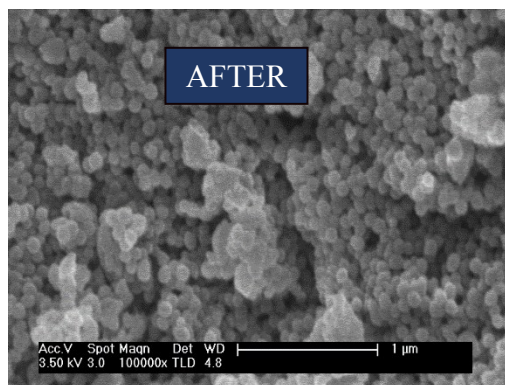
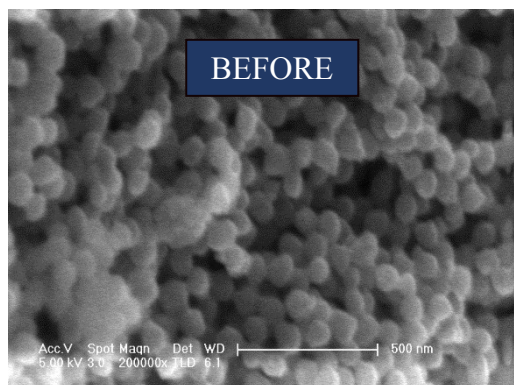
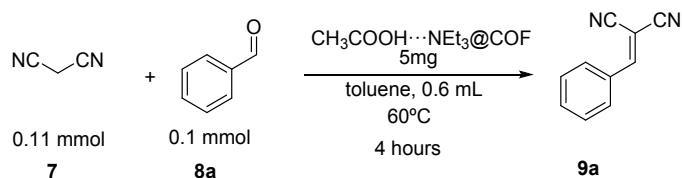


From the SEM images, it can be observed that the morphology of the solid was very different: the COF has been decomposed.

The IR spectra have different signals, which confirms that the solid has been transformed.



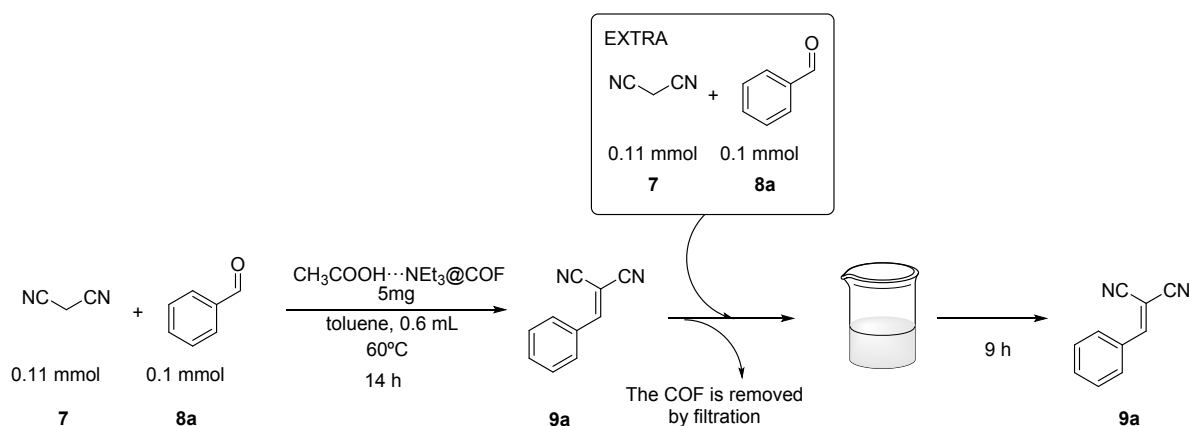
The reaction did not affect the morphology of the COF. The IR spectra show the same signals.



As described in the previous section, $^1\text{H-NMR}$ experiments indicated that malonitrile **7** reacted with the COF and decomposed a part of the material. However, the rest of the COF remained as a solid. From the SEM images and IR spectra, it could be observed that this solid presented the same morphology and the same IR signals.

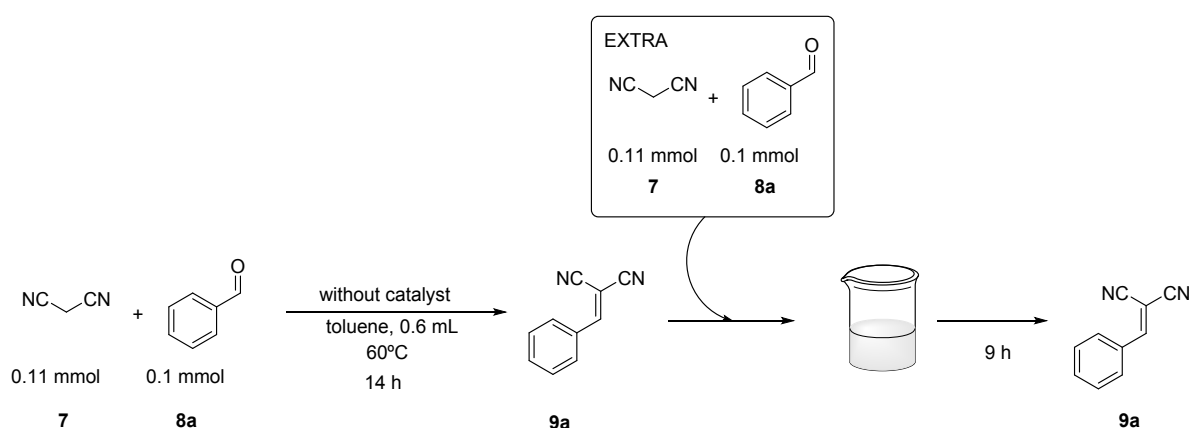
10. Leaching tests

Leaching test of $\text{CH}_3\text{COOH}\cdots\text{NEt}_3\text{@COF}$



The reaction was set up following the general procedure for “Knoevenagel condensation catalyzed by COF” (see above) and the formation of the product **9a** was measured at 14 hours by GC-FID. There was 0.068 mmol of the product **9a** (Yield = 68%).

Then the reaction mixture was filtrated through membrane of 0.45 μm pores in order to remove the COF. Other 0.11 mmol of molonitrile **7** and 0.1 mmol of benzaldehyde **8a** were added to the reaction mixture. The mixture was allowed to react during 9 hours and the formation of the product was measured by GC-FID. There was 0.087 mmol of the product **9a**, therefore, 0.019 mmol had been formed in the second step (Yield in the second step = 19 %)



The same process was repeated but without COF: The reaction was set up following the general procedure for “Knoevenagel condensation catalyzed by COF” (see above) but without adding the COF and the formation of the product was measured at 14 hours by GC-FID. There was 0.008 mmol of the product **9a** (Yield = 8%).

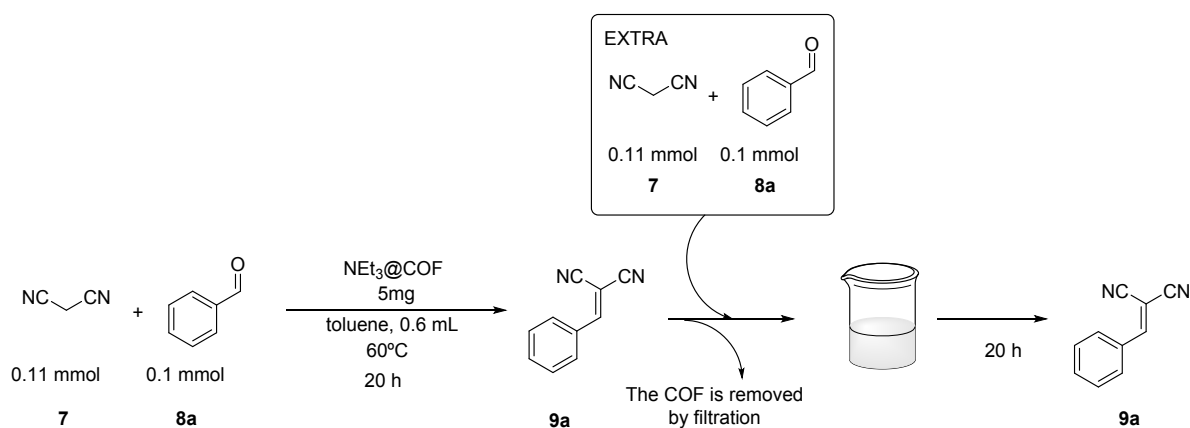
Other 0.11 mmol of molonitrile **7** and 0.1 mmol of benzaldehyde **8a** was added to the reaction mixture. The mixture was allowed to react during 9 hours and the formation of the product was measured by GC-FID. There was 0.012 mmol of the product **9a**, therefore, 0.004 mmol had been formed in the second step (Yield in the second step = 4 %).

In the first experiment, when the $\text{CH}_3\text{COOH}\cdots\text{NEt}_3\text{@COF}$ is presented in the reaction, the yield of the reaction is 68 %, but when the catalytic COF is removed and the reaction is repeated in the reaction media the yield decreases to 19 %. This indicates that the $\text{CH}_3\text{COOH}\cdots\text{NEt}_3\text{@COF}$ acts as a solid heterogeneous catalyst.

However, comparing the second step of the two experiments, we observed that when there is not $\text{CH}_3\text{COOH}\cdots\text{NEt}_3\text{@COF}$ from the beginning, the background reaction in the second step has a yield of 4%.

It can be conclude that the most of the catalytic activity is due to the heterogeneous $\text{CH}_3\text{COOH}\cdots\text{NEt}_3\text{@COF}$.

Leaching test of $\text{NEt}_3\text{@COF}$



The reaction was performed following the general procedure for “Knoevenagel condensation catalyzed by COF” using as catalysis $\text{NEt}_3\text{@COF}$ (see above). The formation of the product **9a** is measured at 14 hours by GC-FID (0.09 mmol of product **9a**, Yield = 90 %) and at 20 hours (0.1 mmol of product **9a**, Yield = 100 %).

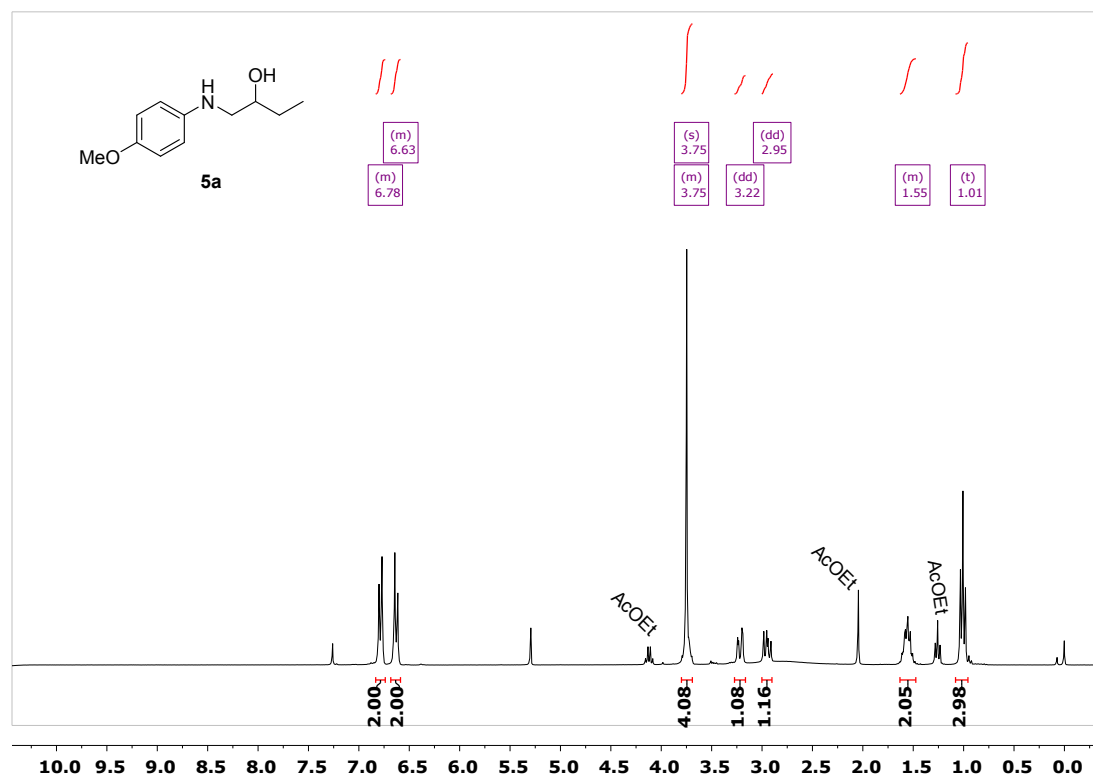
Then, the reaction mixture was filtrated through membrane of 0.45 μm pores in order to remove the COF. Other 0.11 mmol of molonitrile **7** and 0.1 mmol of benzaldehyde **8a** was added to the reaction mixture. The mixture was allowed to react during 20 hours and the formation of the product was measured by GC-FID. There was 0.2 mmol of the product **9a**,

indicating that 0.1 mmol had been formed in the second step (Yield in the second step = 100 %).

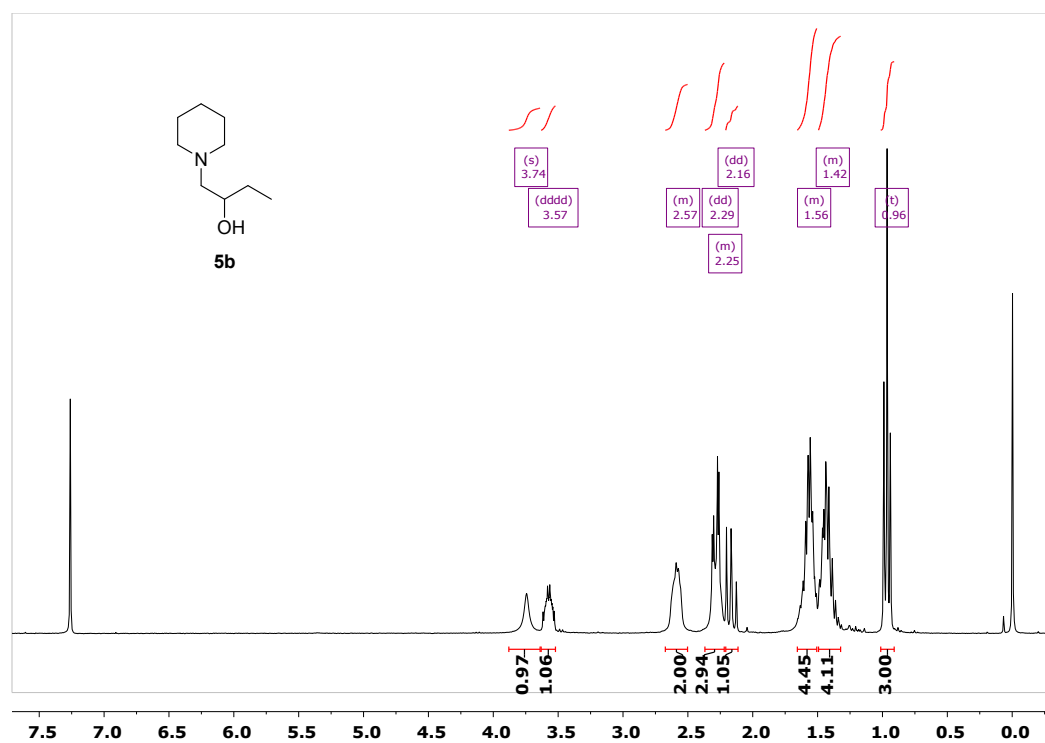
This leaching study indicates that the catalytic activity of **NEt₃@COF** is due to the molecules of Et₃N that are released from the COF and are dissolved in the reaction medium.

11. ¹H-NMR spectra of the products

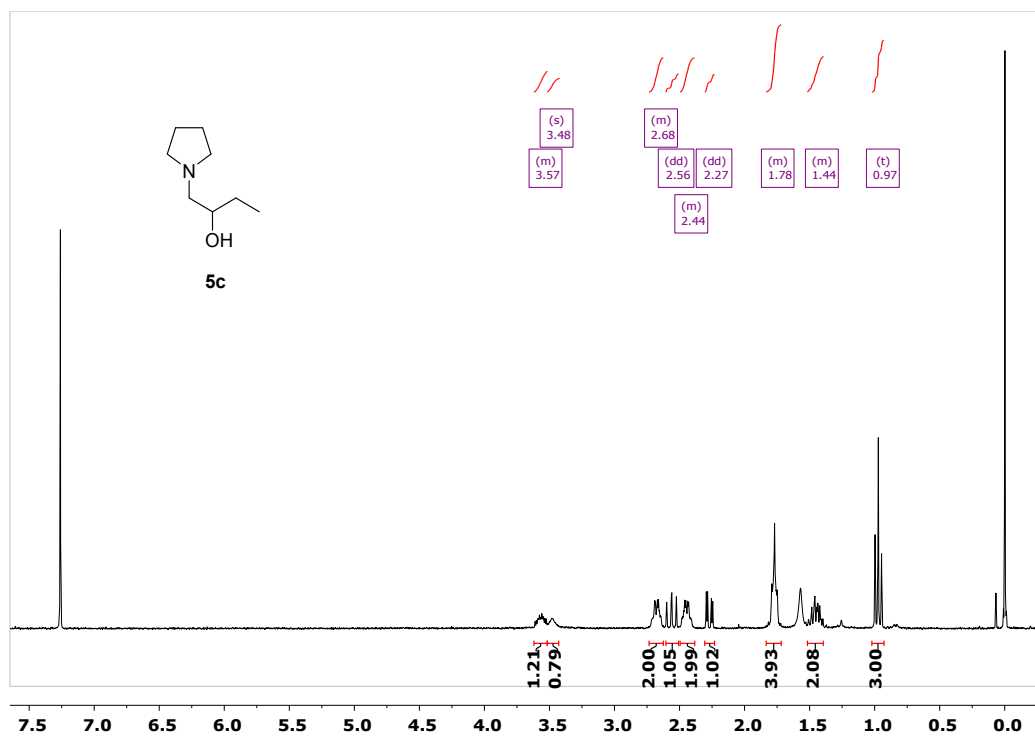
¹H-NMR (CDCl₃, 300 MHz) (5a)



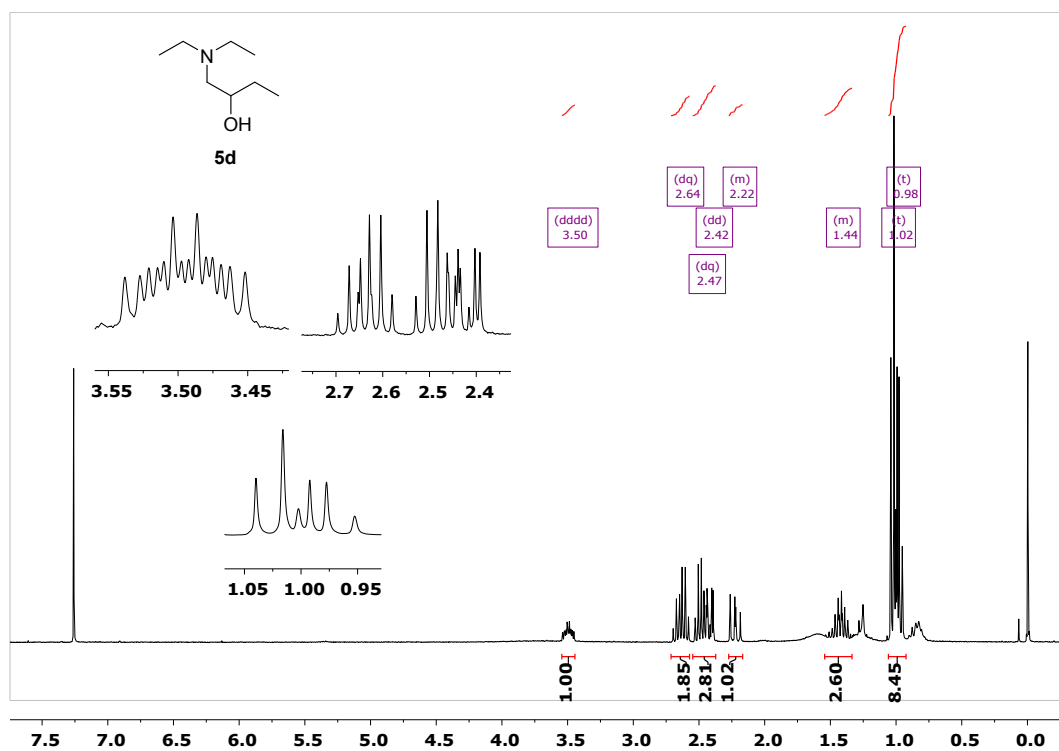
¹H-NMR (CDCl₃, 300 MHz) (5b)



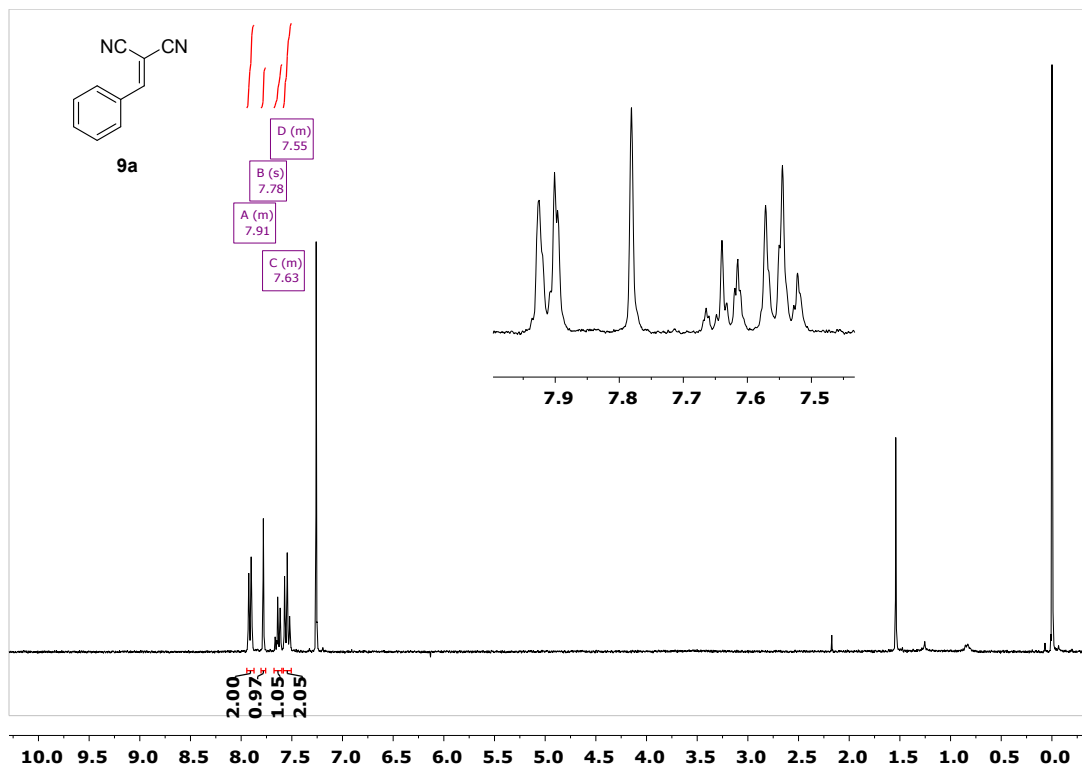
¹H-NMR (CDCl₃, 300 MHz) (5c)



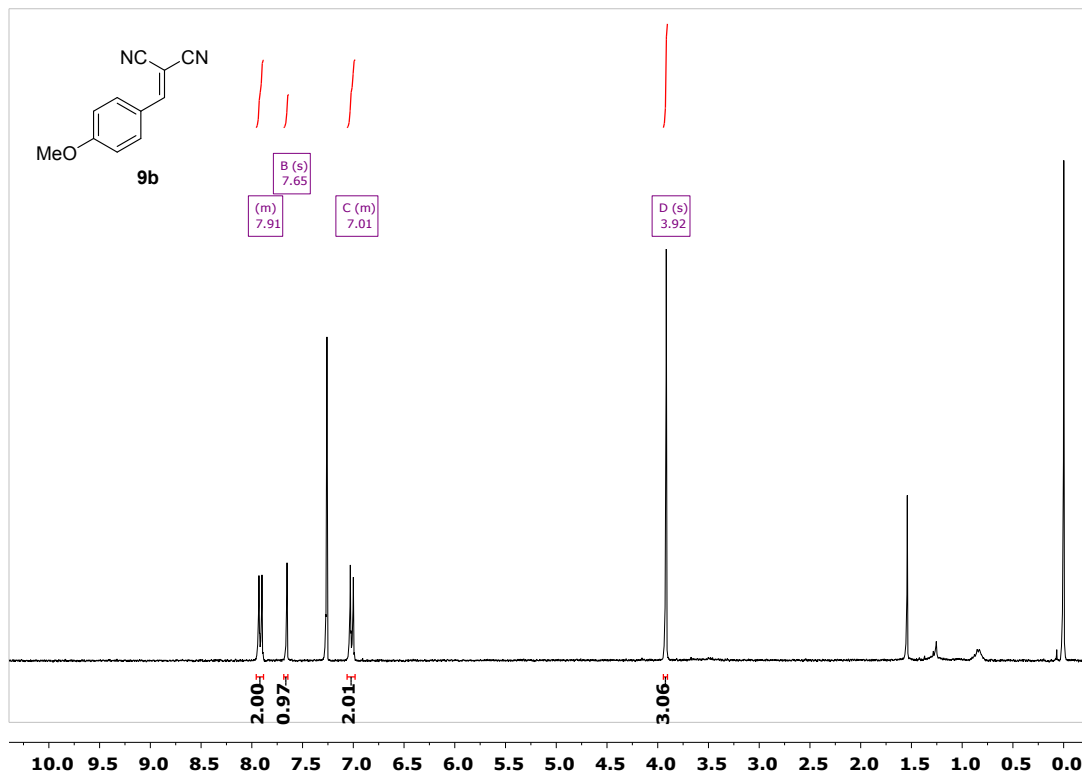
¹H-NMR (CDCl₃, 300 MHz) (5d)



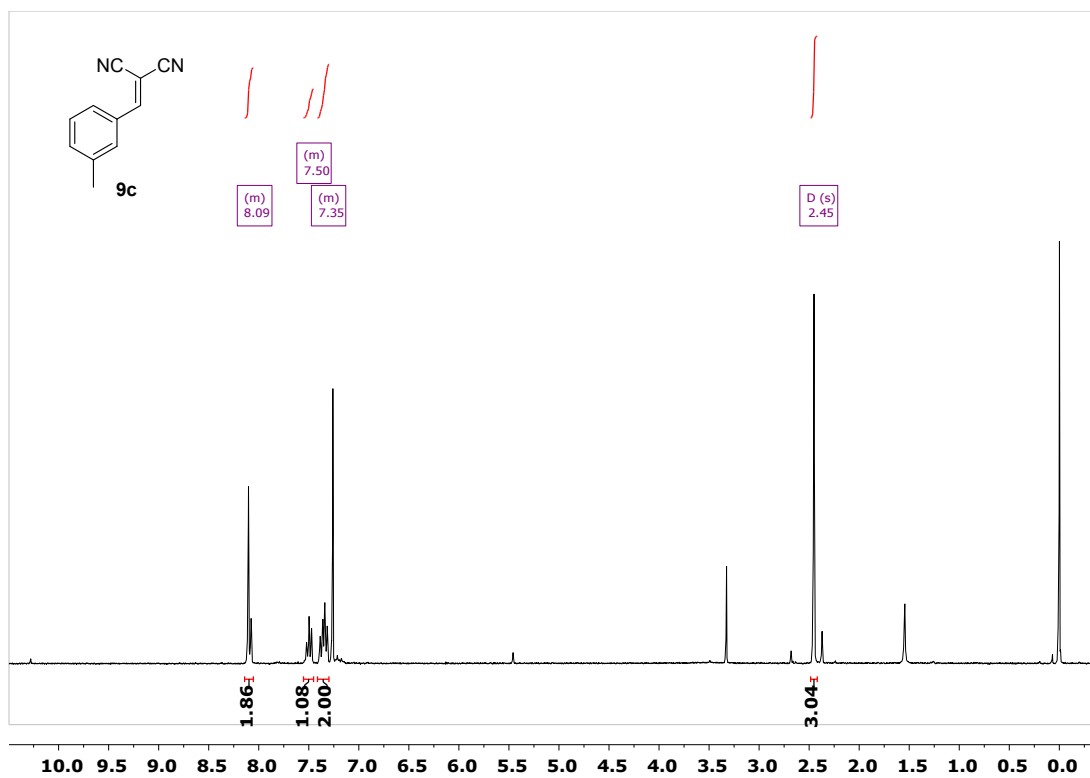
¹H-NMR (CDCl₃, 300 MHz) (9a)



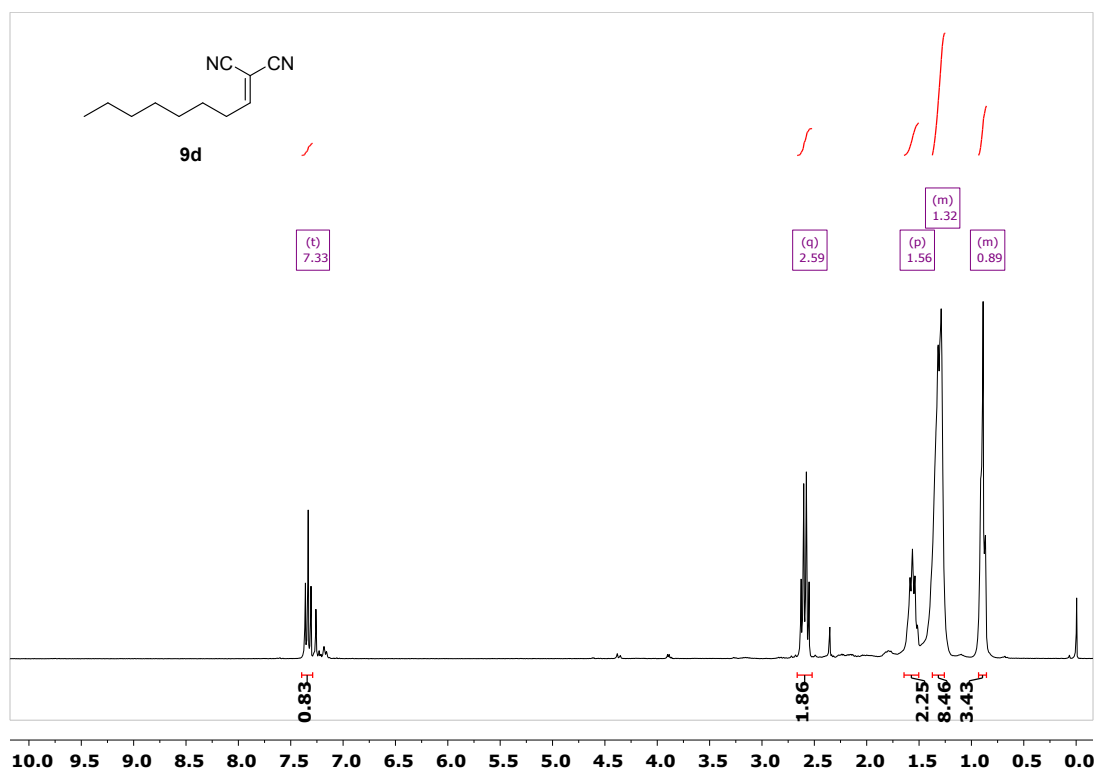
¹H-NMR (CDCl₃, 300 MHz) (9b)



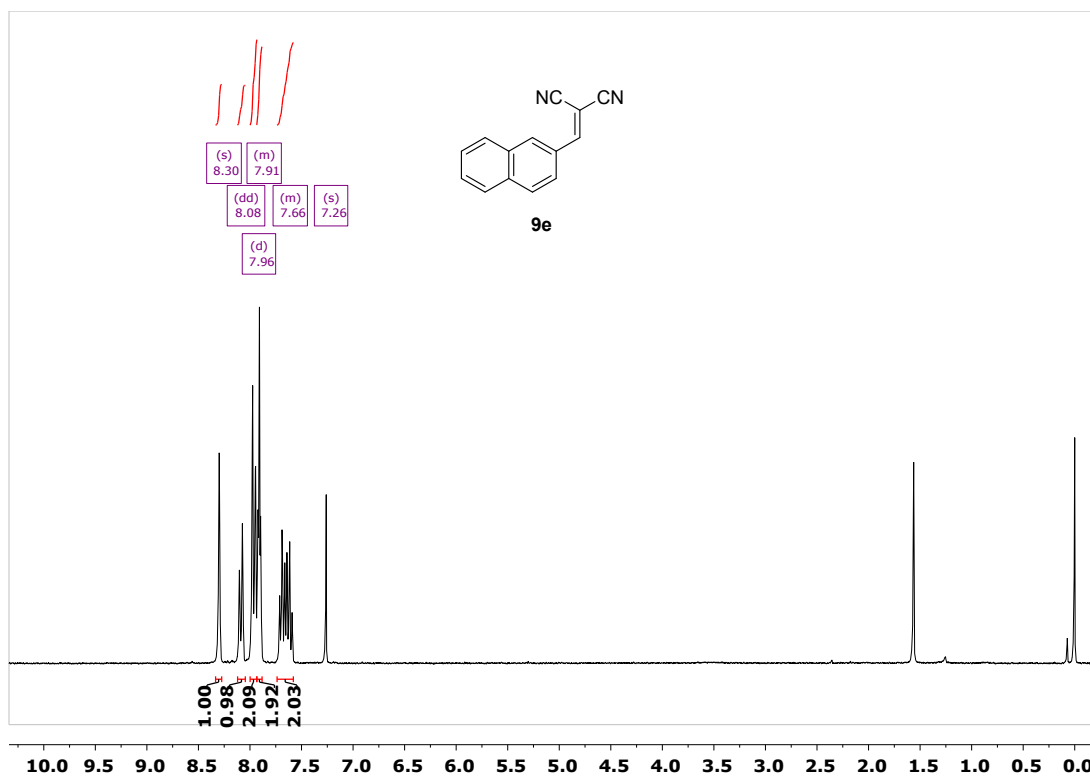
¹H-NMR (CDCl₃, 300 MHz) (9c)



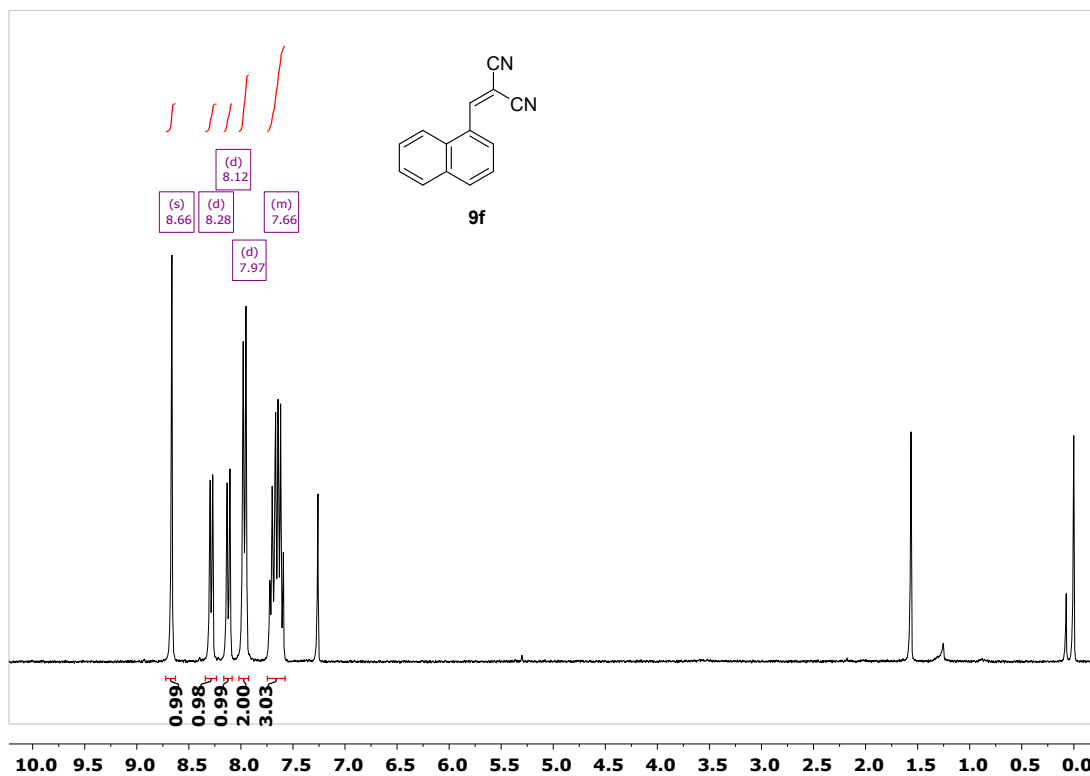
¹H-NMR (CDCl₃, 300 MHz) (9d)



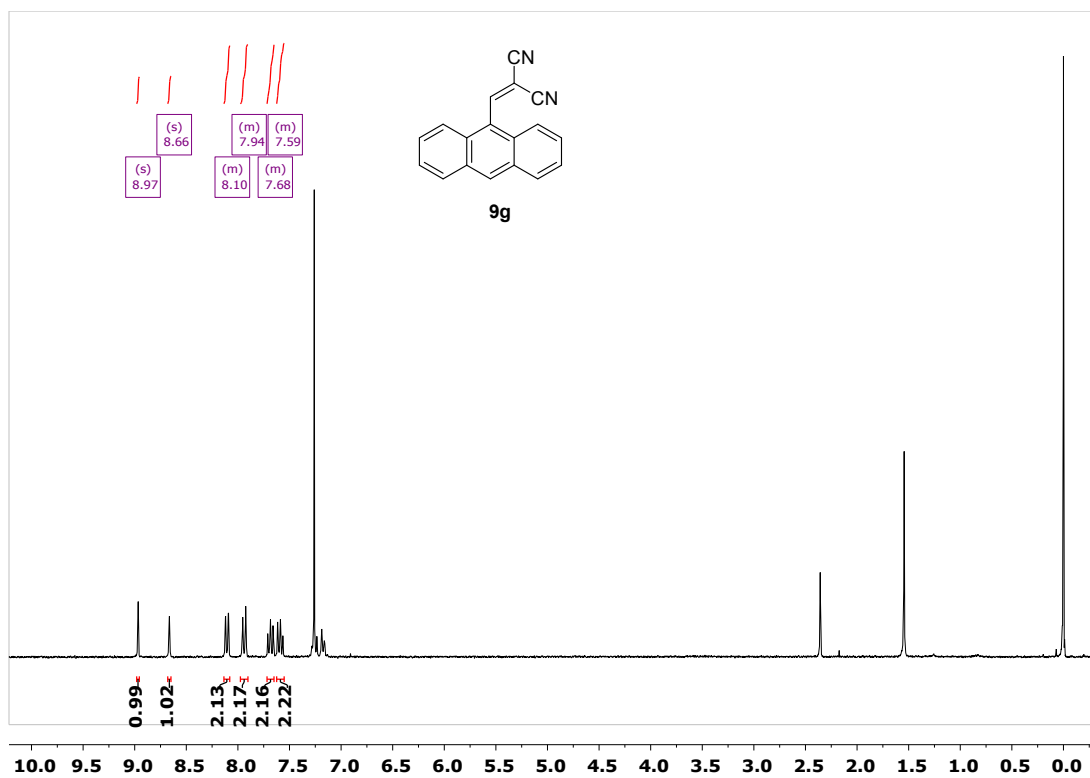
¹H-NMR (CDCl₃, 300 MHz) (9e)



¹H-NMR (CDCl₃, 300 MHz) (9f)



¹H-NMR (CDCl₃, 300 MHz) (9g)



12. Computational details

DFT periodic boundary condition calculations including the whole COF framework have been performed with VASP package.¹¹ These calculations have been used to study the reactivity inside the COF and to characterize the supramolecular interactions between the COF and acetic acid, triethylamine and a system formed by one acetic acid and one triethylamine molecule. The VASP packages uses plane-wave functions for describing the electronic wavefunction and it is very efficient when using GGA functionals. Unfortunately, the computational cost dramatically increases when using hybrid functionals and, in our particular case, the use of hybrid functionals is too expensive. In this context, all periodic calculations have been performed at the PBE level.¹² Dispersion forces were taken into account in the PBE calculations with the Grimme's empirical correction (D2).¹³ We take the advantage that Grimme correction is added a posteriori to the DFT energy to estimate the contribution of the Van der Waals interactions in the global adsorption energies. This estimation is determined as the energy difference between the PBE-D2 and the PBE energies at the PBE-D2 optimized structure. The energy cutoff has been set to 400 eV. Geometry convergence criterion was fix to a change in energy of $1 \cdot 10^{-3}$ eV. The initial structure of the COF has been taken from the literature and the cell parameters ($a = b = 28.127$ Å; $c = 17.758$ Å and $\alpha = \beta = \gamma = 90^\circ$) have been kept constant in all optimizations. All calculations have been performed considering only the gamma point of the reciprocal lattice. Initial structures have been constructed introducing manually the molecular fragments with the geometries obtained with Gaussian09 package. Several different starting points have been considered with the aim of exploring several local minima and analyze the energy difference between them. Several of these different minima are added in the results and discussion section. The differences between them do not change the major results of the computations. Remarkably, the energetics of the transition states have been obtained through a constrained optimization fixing the atoms involved in the formation and breaking of bonds. This imposed that the interatomic distances between the key atoms are kept constant to the values of the transition state obtained with the molecular calculations. This concerns the acidic hydrogen and the oxygen bonded to it of the acetic acid, the oxygen and the less substituted carbon bonded to the oxygen of the epoxide

¹¹ Kresse, G.; Hafner, J. *Phys. Rev. B: Condens. Matter Mater. Phys.* **1993**, *47*, 558–561; Kresse, G.; Hafner, J. *Phys. Rev. B: Condens. Matter Mater. Phys.* **1994**, *49*, 14251–14269; Kresse, G.; Furthmüller, J. *Phys. Rev. B: Condens. Matter Mater. Phys.* **1996**, *54*, 11169–11186; Kresse, G.; Furthmüller, J. *Comput. Mater. Sci.* **1996**, *6*, 15–50.

¹² Perdew, J. P.; Burke, K.; Ernzerhof, M. *Phys. Rev. Lett.* **1996**, *77*, 3865–3868

¹³ S. Grimme, *J. Comput. Chem.* **2004**, *25*, 1463–1473; S. Grimme, *J. Comput. Chem.*, **2006**, *27*, 1787–1799.

and the nitrogen atom of the piperidine in the ring opening reaction as well as the carbonyl carbon of the aldehyde and the central carbon of malononitrile in the Knoevenagel reaction. At this point it is worth mentioning that we have also performed molecular calculations at the PBE-D2/6-311+G(d,p) level of theory with the aim of determining the effect of the functional on the energy barriers. The obtained results are all summarized in Table S1 (see above). Remarkably, the functional choice is crucial in determining the energy barriers, the PBE-D2/6-311+G(d,p) methodology predicting values that are around 40-50 kJ mol⁻¹ lower than those predicted with M06/6-311+G(d,p). This underestimation of the energy barriers is a well-known drawback of pure GGA functionals, which stabilize structures where the electron density is largely delocalized. It is for this reason that we decided to add a correcting factor to the energetics of the species involved in the reactivity inside the COF (reacting precomplex, transition state and product). This correcting factor is determined by the difference between M06 and PBE-D2 values in the relative energies with respect separated reactants of each individual stationary point of the reaction in gas phase. As example, the transition state of the ring epoxide reaction in gas phase is predicted to be 43.5 kJ mol⁻¹ above separated reactants with M06/6-311+G(d,p). The same transition state at PBE/6-311+G(d,p) level of theory is located -8.0 kJ mol⁻¹ with respect to reactants. Therefore, the correcting factor for the energetics inside the COF is 51.5 kJ mol⁻¹.

Table S1. Relative energies in kJ mol⁻¹ of the reactive pre-complex (reactant), transition state (TS) and product of the considered steps summarized in Scheme 4. Values in parenthesis corresponds to Gibbs energies.

Reaction ^[a]	Method	Reactant	TS	Product
1	M06 _(Mol) ^[b]	-59.6 (30.6)	43.5 (144.3)	-15.6 (62.2)
1	M06 _{(Mol)solv} ^[c]	-38.7 (51.1)	35.1 (135.1)	-118.6 (1.1)
1	PBE _(Mol) ^[d]	-70.1 (31.3)	-8.0 (93.9)	-89.0 (34.8)
1	PBE _(PBC) ^[e]	-55.0	17.7	-75.5
2 (8a)	M06 _(Mol) ^[b]	-47.8 (57.4)	-28.9 (89.8)	-101.8 (26.2)
2 (8a)	M06 _{(Mol)solv} ^[c]	-50.3 (56.3)	-24.8 (96.8)	-82.2 (36.3)
2 (8a)	PBE _(Mol) ^[d]	-84.7 (16.4)	-68.5 (48.3)	-119.3 (-2.7)
2 (8a)	PBE _(PBC) ^[e]	-92.5	-91.6	-136.9
2 (8g)	M06 _(Mol) ^[b]	-56.2 (55.8)	-31.4 (87.6)	-110.8 (10.2)
2 (8g)	M06 _{(Mol)solv} ^[c]	-55.8 (56.1)	-24.8 (96.8)	-86.4 (37.7)
2 (8g)	PBE _(Mol) ^[d]	-89.3(15.6)	-68.5 (48.3)	-132.5 (-10.7)
2 (8g)	PBE _(PBC) ^[e]	-117.1	-116.3	-157.0

[a] See Scheme 4 for reaction definition. [b] Molecular gas phase M06/6-311+G(d,p) calculations. [c] Molecular M06/6-311+G(d,p) calculations including solvent effects with implicit models [d] Molecular gas phase PBE-D2/6-311+G(d,p) calculations. [e] PBE-D2 periodic boundary conditions calculations including the whole COF framework.

12. 1. DFT calculations for the imine structure-adsorbed molecules interactions

Results are presented in **Figure 4** in the manuscript, showing the optimized geometries, selected geometrical parameters and the adsorption energies of these imine structures functionalized with CH_3COOH , NEt_3 and $\text{CH}_3\text{COOH}\cdots\text{NEt}_3$ adducts. At this point, it is worth mentioning that we explored a limited number of relative orientations between the imine structure and the adsorbed molecule, as well as different conformations of the adsorbed molecules. The computed adsorption energies did not present large differences and therefore, we assumed that main trends would be conserved, even if more favorable minima were overlooked.

The interaction between acetic acid and the imine structure is established through hydrogen bonding between the acidic proton of the acetic acid and the imine group of the structure (**Figure 4**, top). The $\text{OH}\cdots\text{N}$ distance is 1.66 Å, which is indicative of a strong hydrogen bond. The associated adsorption energy is $-79.4 \text{ kJ mol}^{-1}$.

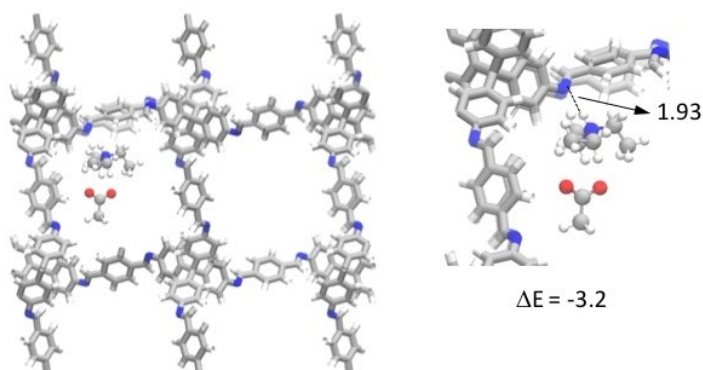
On the other hand, the imine of the structure and the adsorbed amine (NEt_3) are both basic and no hydrogen bonding is possible between them. In this context, the adsorption takes place only through Van der Waals interactions and the preferred structure presents the NEt_3 close to the walls of the imine material. The shortest distances between atoms of NEt_3 and those of the imine structure are smaller than 4 Å (**Figure 4**, middle). The resulting adsorption energy is $-43.6 \text{ kJ mol}^{-1}$.

Finally, we studied the interaction of the $\text{CH}_3\text{COOH}\cdots\text{NEt}_3$ mixture with the imine structure, considering a 1 to 1 relationship between CH_3COOH and NEt_3 (**Figure 6**, middle). Three possibilities were considered (see **Figure 4** and S22): *a*) The interaction between CH_3COOH and the imine structure through hydrogen bonding with the presence of a NEt_3 molecule in the channel; *b*) The formation of a $\text{CH}_3\text{COOH}\cdots\text{NEt}_3$ complex interacting with the imine structure through Van der Waals interactions; and *c*) The interaction between a protonated triethylammonium ion with the imine group of the structure through hydrogen bonding and an acetate anion inside the channel.^[14]

¹⁴ In this latter case, we also explored the possibility of an ion pair formation $\text{CH}_3\text{COO}\cdots^+\text{HNEt}_3$, but the optimization evolved to the structure without charge separation.

NEt₃⋯CH₃COOH@COF Adducts

Triethylammonium interacting with the COF



NEt₃⋯CH₃COOH aggregate in the middle of the channel

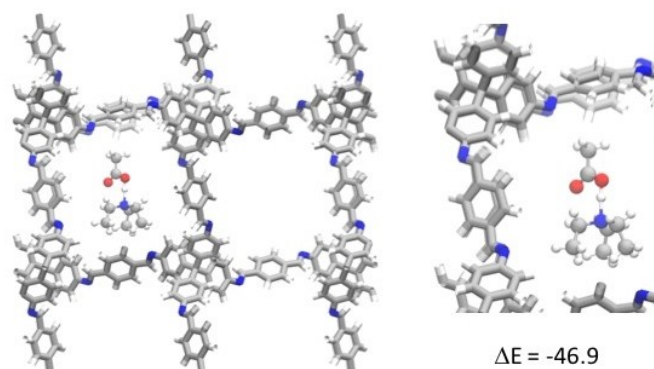


Figure S22. Optimized geometries of the NEt₃⋯CH₃COOH@COF adducts not reported in the main text and their adsorption energies (ΔE) with respect to the NEt₃⋯CH₃COOH desorption. Distances are in Å and energies in kJ mol⁻¹.

Within these initial structures, possibilities *a*) and *b*) almost equally raised as the most favorable situations. The first one can be described as an CH₃COOH molecule interacting with the imine structure through hydrogen bonding, while the remaining NEt₃ molecule interacts with the imine structure and CH₃COOH through van der Waals interactions. Such structure presents a strong N⋯HO hydrogen bond as evidenced by a short distance of around 1.52 Å. The second one implies the formation of a neutral CH₃COOH⋯NEt₃ aggregate, interacting with the imine structure through van der Waals interactions, being the shortest distances between the guest molecules and the imine structure around 2.5 Å (**Figure 4**, bottom). Therefore, the mixture CH₃COOH + NEt₃ in the imine structure shows a combination of intermolecular and

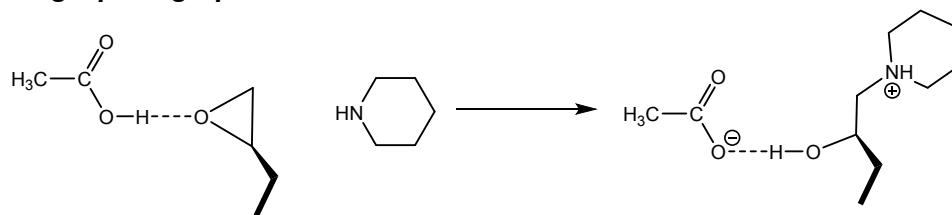
molecule-imine structure interactions that enhance the adsorption of the base molecule. For this material, we evaluated the thermodynamic cost of leaching one molecule of NEt_3 (47 kJ mol^{-1}) or the whole $\text{CH}_3\text{COOH}\cdots\text{NEt}_3$ aggregate (59.5 kJ mol^{-1}). Therefore, the most probable leaching process will correspond to the liberation of NEt_3 from **$\text{CH}_3\text{COOH}\cdots\text{NEt}_3@a-3/c-3$** .

Overall, the computed adsorption energies suggested that NEt_3 will be more easily released from the imine structure when no CH_3COOH is present in the material (by 15.9 kJ mol^{-1}). Moreover, CH_3COOH in **$\text{CH}_3\text{COOH}@a-3/c-3$** was adsorbed more strongly than $\text{CH}_3\text{COOH}\cdots\text{NEt}_3$ aggregate in **$\text{NEt}_3\cdots\text{CH}_3\text{COOH}@a-3/c-3$** , suggesting that their removal would require harder conditions.

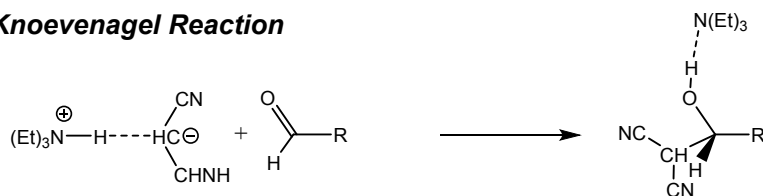
12.2. Analysis of Influence of Confinement of the Active Site by DFT Calculations

With the aim of further analysing the influence of the imine structure in the catalytic processes, we performed DFT calculations of the ring opening epoxide reaction catalysed by **$\text{CH}_3\text{COOH}@a-3/c-3$** and the Knoevenagel reaction catalysed by **$\text{CH}_3\text{COOH}\cdots\text{NEt}_3@a-3/c-3$** . Although CH_3COOH is needed to prevent NEt_3 leaching in the latter process, the base is the active catalytic centre. Therefore, we did not include CH_3COOH in the modelling in order to decrease the computational cost. The computational study was focused on understanding if the reaction can take place in a cavity defined by the imine structure as well as on determining the possible origin of the size selectivity. For that, we considered both the molecular systems and calculations with periodic boundary conditions, including the whole imine structure (see S. I., section 11 for the computational details). In each reaction, we explored the elementary step in which the new C-N or C-C bonds are formed (**S23**), assuming that the protonation/deprotonation steps as well as those for dehydration would be kinetically easier.

Ring-Opening-Epoxyde



Knoevenagel Reaction



8a R = Ph

8g R =

Figure S23. Reaction steps studied computationally for the epoxide ring opening and Knoevenagel reactions.

12.2.1. Ring-Opening-Epoxyde and Knoevenagel Reactions

Regarding to the homogenous conditions, M06 calculations in gas phase and solution suggested that the reaction is concerted and once the epoxide ring is opened, the C-N bond is formed, and the proton of CH₃COOH is simultaneously transferred to the geminal alkoxide (see **S23** and **S24**). In solution, this concerted process is exothermic in terms of potential energy (-118.6 kJ mol⁻¹) and it presents a relatively low energy barrier of 73.8 kJ mol⁻¹ with respect to the reactants together forming the initial complex (**S25**). It is worth mentioning that the main difficulty to perform the reaction is to approach the three reactants. Indeed, entropic effects are highly unfavourable and once thermal corrections are considered, the energy barrier becomes significantly higher ($\Delta G^\ddagger = 135.1$ kJ mol⁻¹, see S.I.).

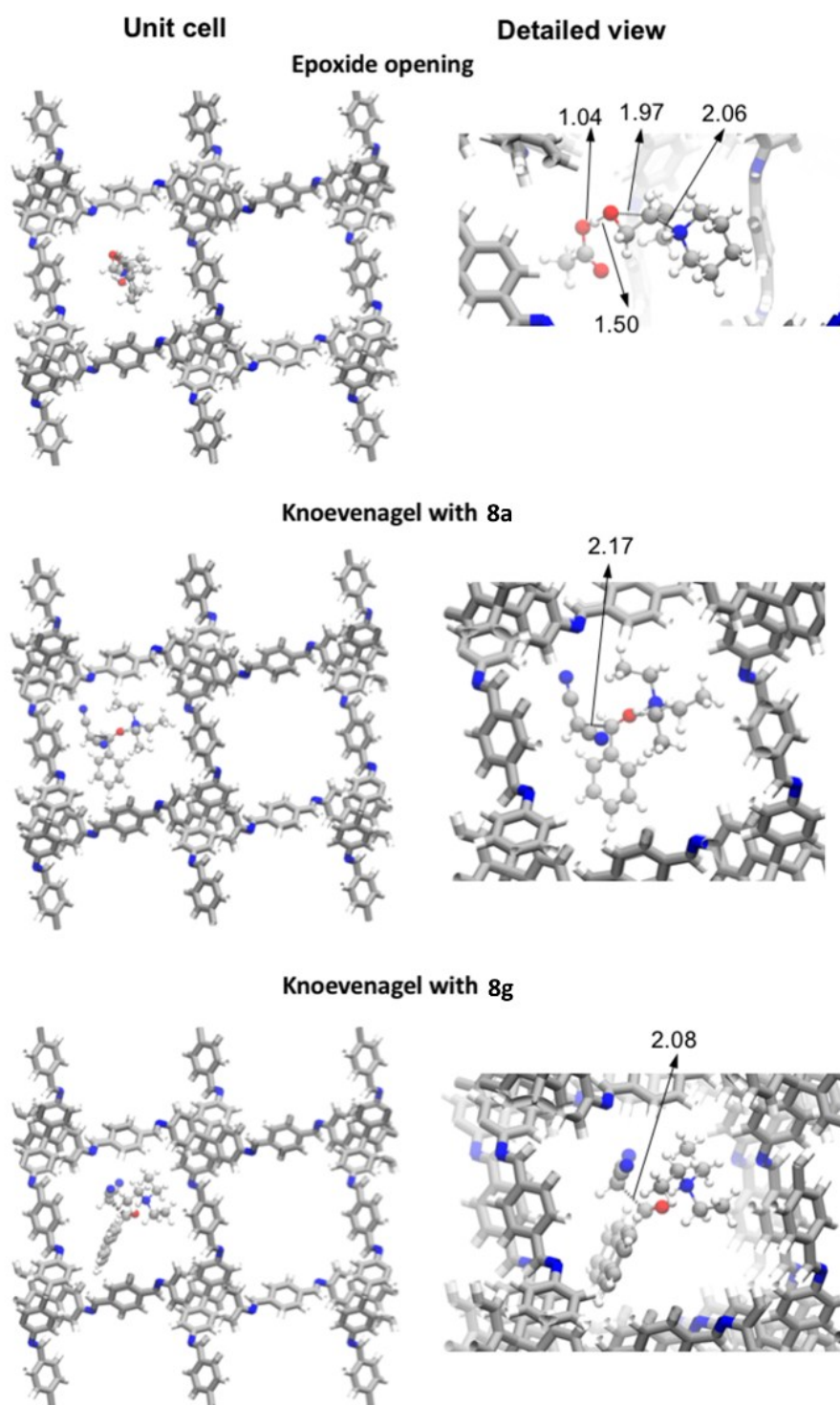
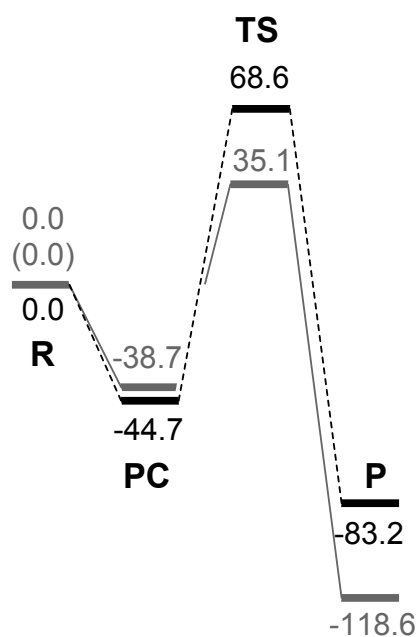
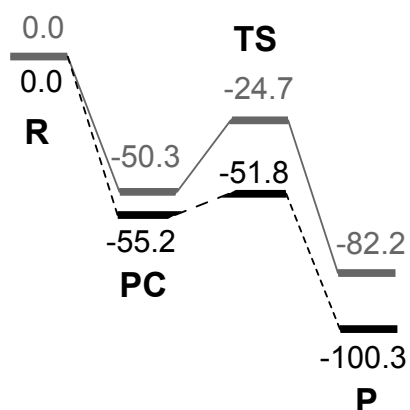


Figure S24. Optimized structures of the transition states associated to the ring opening epoxide and Knoevenagel reactions in the cavity defined by the imine structure. All distances are in Åstrongs.

a) Ring-Opening-epoxide



b) Knoevenagel with 8a



c) Knoevenagel with 8g

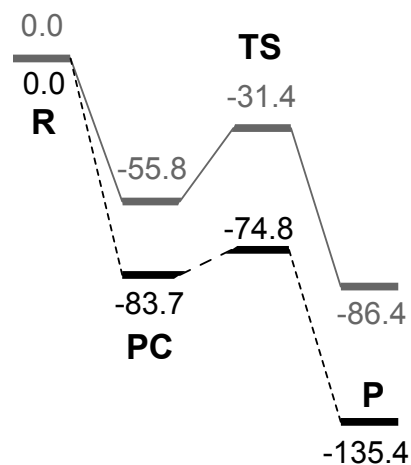


Figure S25. Energy profile in kJ mol⁻¹ of Ring-Opening-Epoxide (a) and Knoevenagel with **8a** (b) and **8g** (c). Grey curves correspond to the M06/6-311+G(d,p) values associated with reaction in solution, while values in black correspond to the best estimated values for the reactions inside a cavity defined by the imine structure. **R** stands for separated reactants, **PC** for the reacting precomplex, **TS** for transition state and **P** for the products of the elementary step considered.

Inclusion of the imine structure has little influence on the reaction energetics. Comparison between the molecular M06 values with those obtained with the best estimation considering the whole materials show little differences. In general, the imine structure marginally destabilizes the transition state. This suggests that the process would be slightly more energetically demanding inside the channels than in solution, but the computed energy barriers agree well with a feasible process requiring heating and large reaction times. The analysis of the structure of the transition state in the imine structure (**S24**) shows that the transition state perfectly fits inside the channel. The imine structure is around 4-5 Å far from the reacting species. Moreover, it suggests that cyclic secondary amines should in general react inside the imine structure, since their width (< 5 Å in the case of piperidine) is significantly smaller than the section of the cavity defined by the imine structure (around 11 Å).

Epoxide Ring Opening reaction

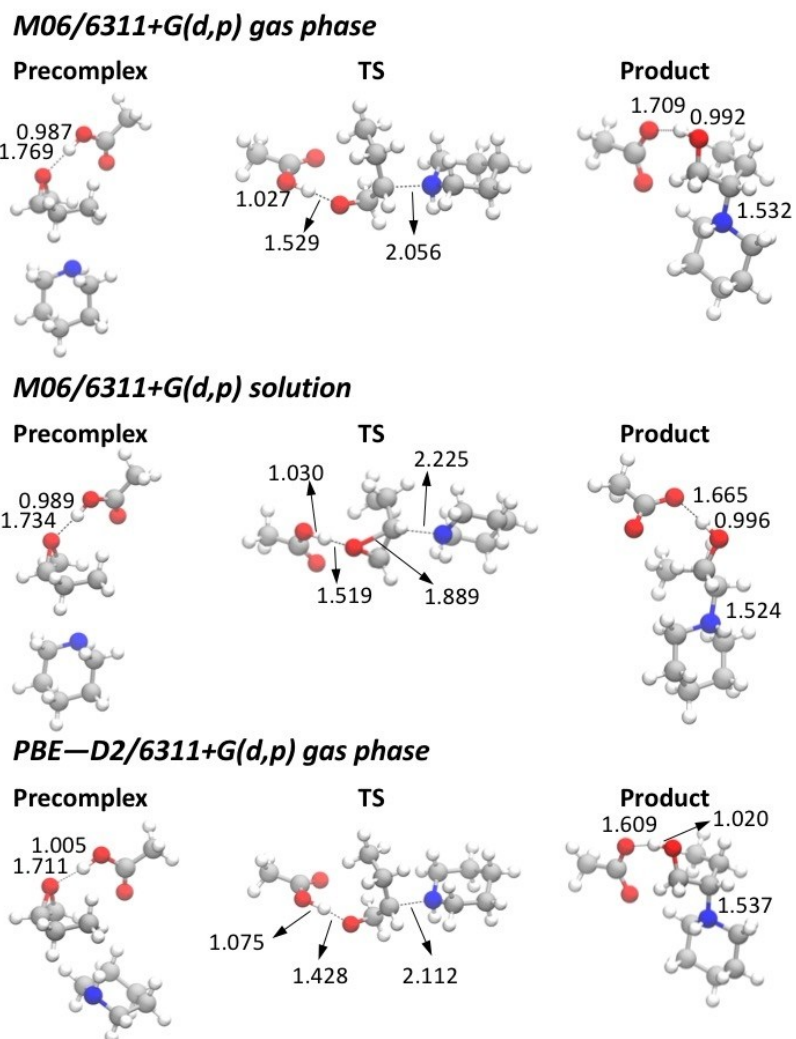
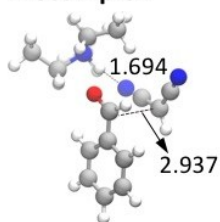


Figure S26. Optimized geometries of all intermediates and transition states found for the epoxide ring opening reaction involving **3b**. All distances are in Å.

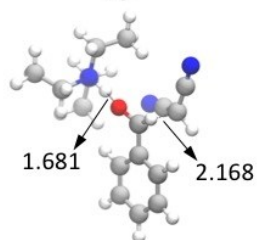
Knoevenagel reaction with 8a

M06/6311+G(d,p) gas phase

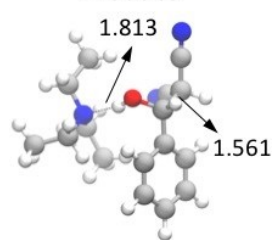
Precomplex



TS

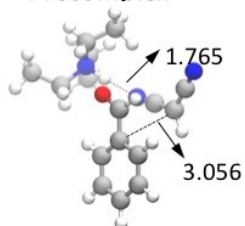


Product

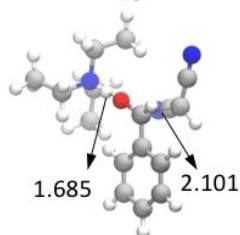


M06/6311+G(d,p) solution

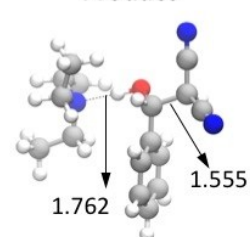
Precomplex



TS

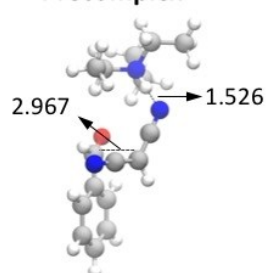


Product

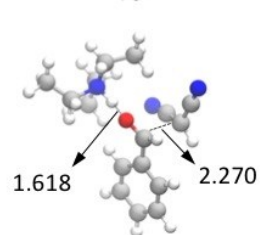


PBE-D2/6311+G(d,p) solution

Precomplex



TS



Product

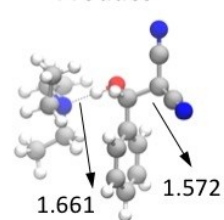
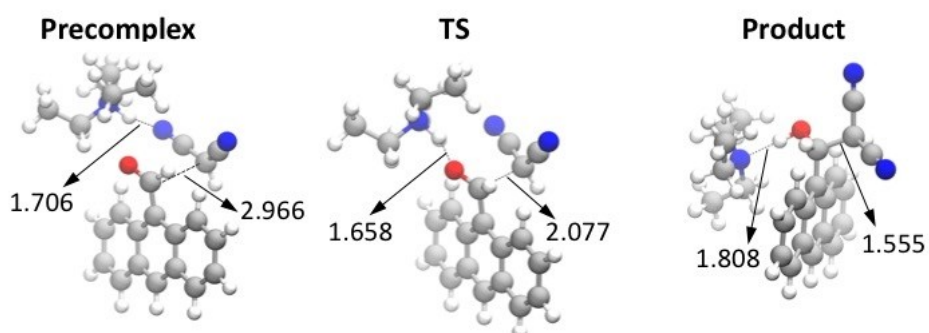


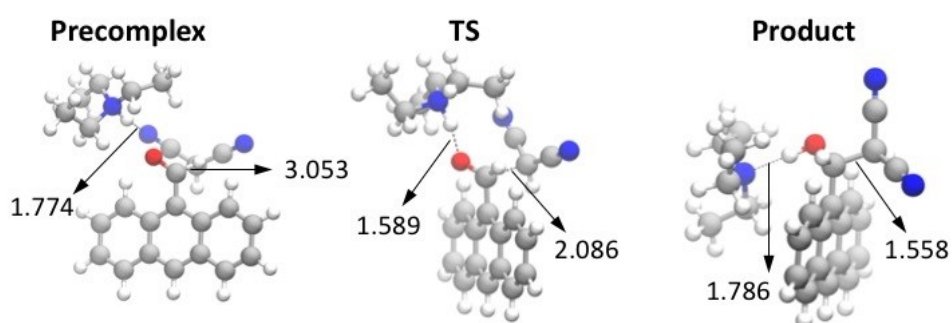
Figure S27. Optimized geometries of all intermediates and transition states found for the Knoevenagel reaction involving **8a**. All distances are in Å.

Knoevenagel reaction with **8g**

M06/6311+G(d,p) gas phase



M06/6311+G(d,p) solution



PBE-D2/6311+G(d,p) solution

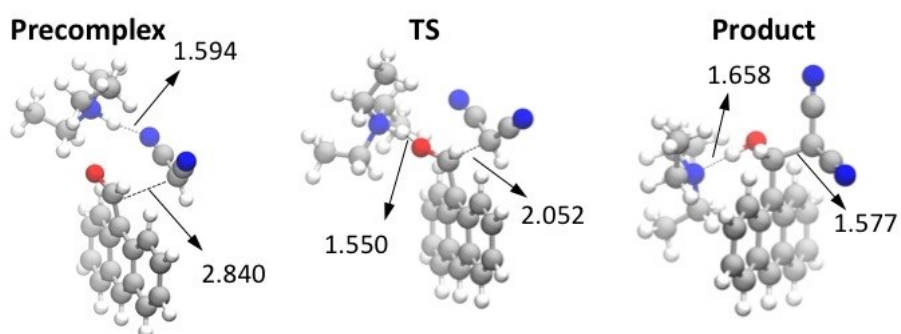
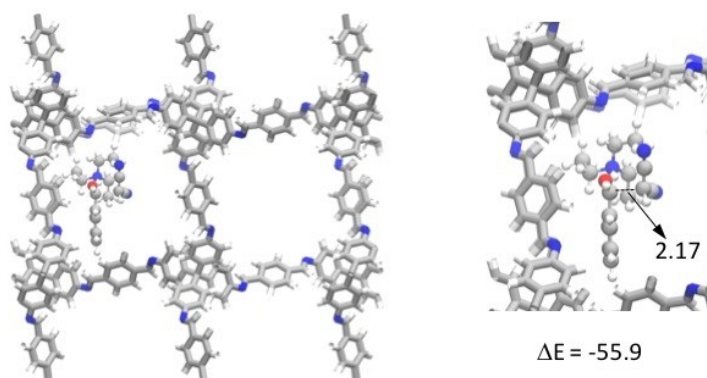


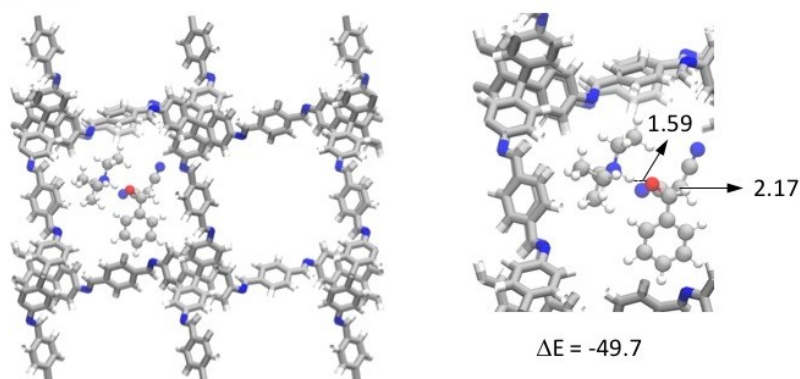
Figure S28. Optimized geometries of all intermediates and transition states found for the Knoevenagel reaction involving **8g**. All distances are in Å.

Additional Transition states Knoevenagel reaction

TS'-8a



TS''-8a



TS'-8g

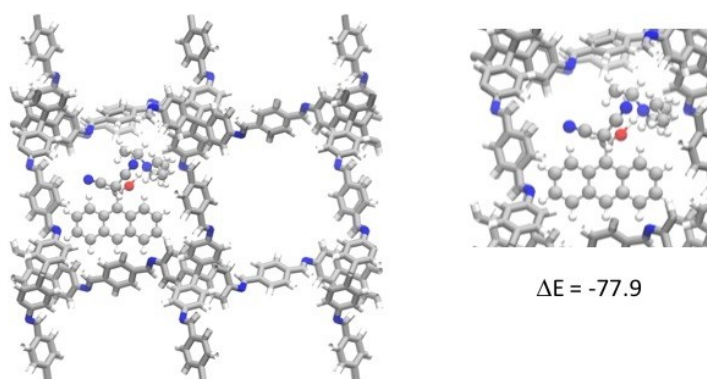


Figure S29. Optimized geometries of the transition states associated with the Knoevenagel reaction either with **8a** or **8g** not reported in the main text and their relative energies (ΔE) with respect to reactants ($\text{NEt}_3\text{@COF} + \text{CH}_2(\text{CN})_2 + \text{RCHO}$). Distances are in Å and energies in kJ mol^{-1} .

12.3. Stability of a-3 and derivatized materials under the reaction conditions: Disassembly pathways

In addition to the reactions shown above, we carried out the reaction between *para*-methoxyaniline (**4d**) and ethyl epoxide **5** (**S30**).^[15] When **CH₃COOH@a-3** was used as catalyst, this reaction resulted on selective formation of mono-substituted product **6d** in a low yield (20 %). This low yield was due to the disassembly of **CH₃COOH@a-3**, as we detected the formation of the corresponding imine **10** in the crude mixture. Indeed, a strong change in the morphology of **CH₃COOH@a-3** was found by SEM (see bottom, **S30** and compare with **S4**). The fact that the catalytic activity was stopped because of the disassembly of material was a clear indication that catalysis depended on the integrity of **CH₃COOH@a-3**. Therefore, **CH₃COOH** molecules act as catalytic centres only when they are associated to the porous framework, otherwise they easily vaporise.

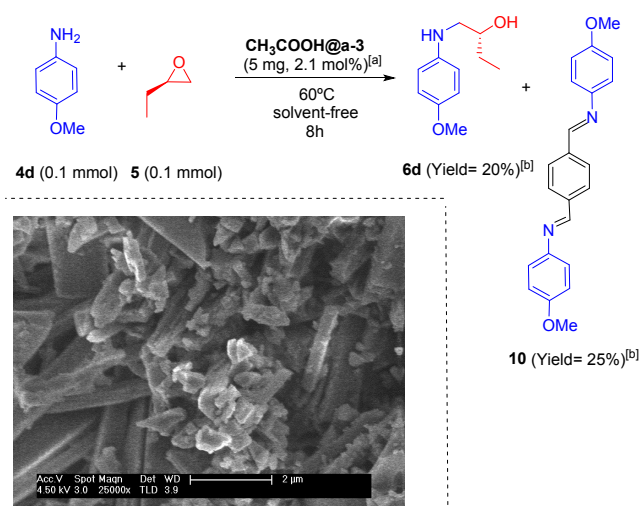


Figure S30. Initial ring opening epoxide explored in this work catalysed by **CH₃COOH@a-3**. Inset shows SEM image of the solid residue after the catalytic run. ^[a] mol% obtained from TGA analysis (2.57% of total mass). ^[b]Yield related to the consumption of **4d**.

In the quest to obtain further insights on the reasons for the scarce yield obtained in the reaction between ethyl epoxide and methoxy aniline (**S30**), we examined the stability of **CH₃COOH@a-3** towards the aniline, secondary amine and epoxide reagents. Epoxide reagent **5** did not show any reactivity with **CH₃COOH@a-3**

¹⁵ We carried out this reaction, using as a catalyst the **CH₃COOH@COF** under the conditions that we found optimal for epoxide-ring opening by reaction with aniline catalyzed by MOF containing squaramides (solventless at 60 °C). See: C. Vignatti, J. Luis-Barrera, V. Guillerm, I. Imaz, R. Mas-Balleste, J. Alemán, D. Maspocho, *ChemCatChem*, 2018, DOI: 10.1002/cctc.201801127.

(Equation a, **S31**), whereas methoxyaniline **4d** decomposed the imine structure through nucleophilic attack, resulting in the formation of a molecular diimine **10** (Equation b, **S31**). Such decomposition was followed by the presence of a $^1\text{H-NMR}$ signal in CDCl_3 at 8.54 ppm (due to $\text{N}=\text{CH-}$ protons). In contrast, the secondary amine did not react at all (Equation c, **S31**).

We extended this evaluation to the reaction conditions of a typical Knoevenagel condensation. To this end, we analysed the stability of $\text{CH}_3\text{COOH}\cdots\text{NEt}_3@a-3$ towards malononitrile (**7**) and benzaldehyde (**8a**) (Equation d and e, **S31**). While benzaldehyde reagent was inert towards the imine structure, malononitrile reacted with it through nucleophilic attack (Equation e). The generation of the molecular product from such decomposition was also followed by the presence of the $^1\text{H-NMR}$ signals in CDCl_3 at 8.05 and 7.82 ppm (C_6H_4 ring and $(\text{CN})_2\text{C}=\text{CH-}$ proton, respectively, see S. I., section 7).

The results presented above clearly indicated that **a-3** was reactive in presence of strong nucleophiles (**7** and **4d**) producing stable products. Therefore, imine structures are sensitive to the nucleophilic attack that result in erosion of the organic framework as a consequence of the reversible nature of the imine bond. Such decomposition reactivity competes with the catalysed reaction. Thus, in the case of Knoevenagel reactions, catalytic conditions (excess of aldehyde with respect to material) disfavour such reactivity. Indeed, examination by $^1\text{H-NMR}$ of the reaction mixture between benzaldehyde and malononitrile revealed that, while 5% of malononitrile reacted with the catalytic material (which corresponds to a 14% of the material), the remaining 95% of such substrate reacted with the benzaldehyde to produce the expected Knoevenagel product **9a**. Nevertheless, imine structure reactivity limits the output of the catalytic reaction and the recyclability of the corresponding material.

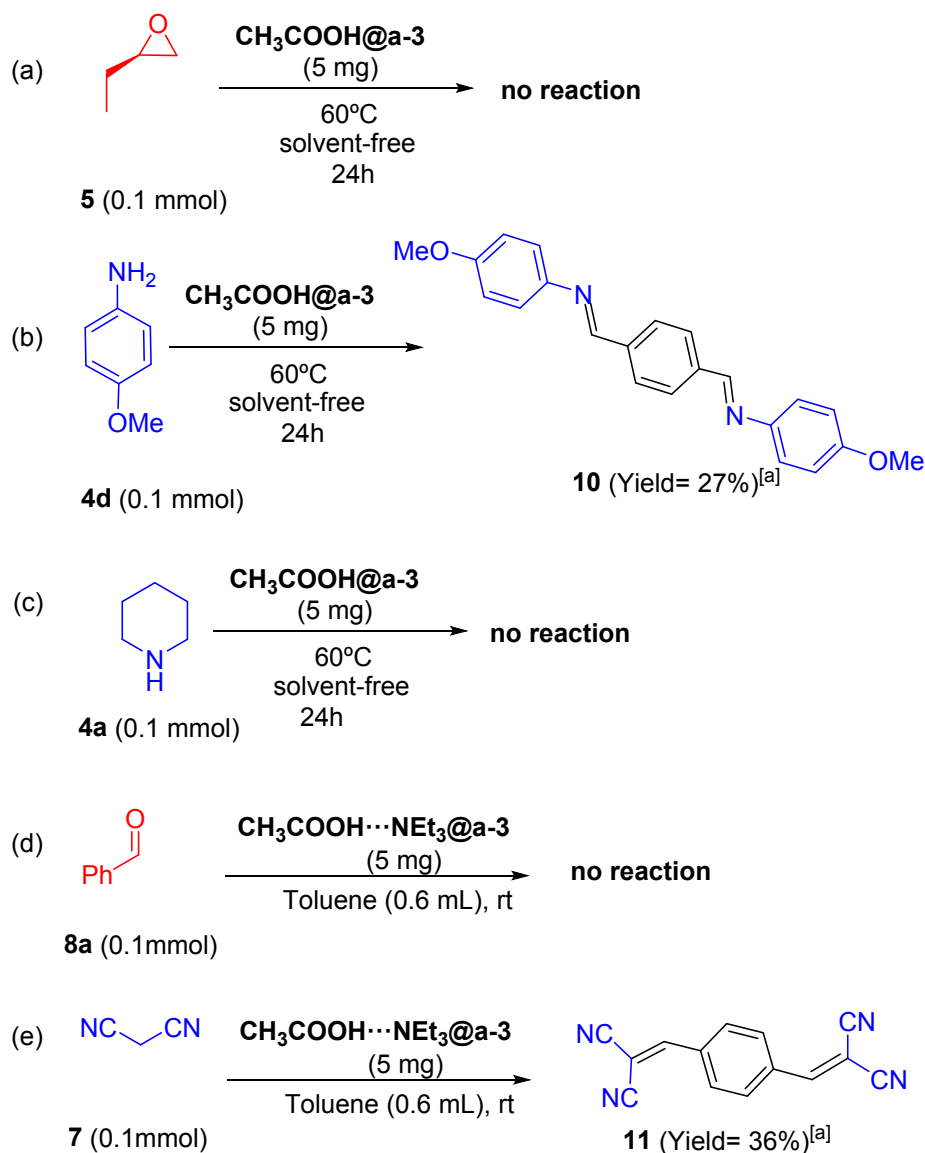


Figure S31. Stability studies performed on catalytically active **a-3** used in this work. ^[a] NMR yield related to decomposed material being other reagents in large excess.

Two sets of calculations have been performed to analyze computationally the interactions between acetic acid, triethylamine and the COF as well as the catalytic activity of the resulting material in the epoxide ring opening and the Knoevenagel reactions. On one hand, M06/6-311+G(d,p) molecular calculations have been performed with Gaussian09 package.¹⁶ With these calculations we have explored the energetics of the studied reactions in gas phase and solution. Vibrational analysis has been used to ensure the nature of the stationary points (minima or transition state). Thermal effects have been computed assuming an ideal gas, the rigid rotor approximation and harmonic frequencies at $T = 298\text{ K}$ and $P = 1\text{ atm}$. In addition, solvent effects have been included with the SMD implicit model.¹⁷ For the case of the epoxide

¹⁶ Y. Zhao, D. G. Truhlar, *Theor. Chem. Acc.* **2008**, *120*, 215; Hariharan, P. C.; Pople, J. A. *Theor. Chim. Acta* **1973**, *28*, 213–222; Frisch, M. J. et al. Gaussian09.

ring opening reaction, dichloromethane ($\epsilon = 8.93$) have been used as solvent since its dielectric constant is in between that of piperidine ($\epsilon = 5.6$) and several epoxides ($\epsilon = 14.0$ for ethylene oxide). In the Knoevenagel reaction, solvent effects are included considering the dielectric constant of toluene; the solvent used in experiments.

¹⁷ A. V. Marenich, C. J. Cramer, D. G. Truhlar, *J. Phys. Chem. B* **2009**, *113*, 6378.